Chemical and Process Engineering: New Frontiers, 2026, 47(2), e135
DOI: 10.24425/cpe.2026.158133

PERSPECTIVE ARTICLE

Hydrogen and syngas production from methane via thermochemical conversion: a mini review of artificial neural network applications

Robert Cherbański*, Tomasz Kotkowski, Eugeniusz Molga

Warsaw University of Technology, Faculty of Chemical and Process Engineering, Waryńskiego 1, Warsaw, Poland

*** Corresponding author, e-mail:** robert.cherbanski@pw.edu.pl

Chemical Engineering Horizons and Perspectives Article series endorsed by the Scientific Committee on Chemical and Process Engineering of the Polish Academy of Sciences, 2024–2027.

Article info:
Received: 02 April 2026
Revised: 06 May 2026
Accepted: 14 May 2026

Abstract
This mini-review examines the application of artificial neural networks (ANNs) in hydrogen and syngas production from methane via thermochemical conversion processes, including steam methane reforming, dry reforming, methane pyrolysis and partial oxidation of methane. These processes involve complex interactions between thermodynamics, reaction kinetics and transport phenomena. In particular, gaps in the understanding of reaction kinetics limit the effectiveness of conventional modelling approaches. This review highlights how ANNs, particularly multilayer perceptron (MLP) and radial basis function (RBF) networks, provide efficient data-driven alternatives for modelling thermodynamic equilibrium, reaction kinetics, catalyst deactivation (coking and poisoning) and reactor performance. Reported studies demonstrate that ANNs can achieve high predictive accuracy, often outperforming simplified empirical models while significantly reducing computational cost. The influence of key operating variables, such as temperature and feed composition, is identified as critical for process performance. Recent advances emphasize hybrid approaches integrating ANNs with first-principles models, computational fluid dynamics, and microkinetic simulations, including physics-informed and physics-enhanced neural networks. Despite promising results, challenges remain related to limited datasets and model interpretability.

Keywords
artificial neural networks, methane reforming, methane pyrolysis, hydrogen, syngas

1. INTRODUCTION

Carbon dioxide (CO_2) and methane (CH_4) are the two major greenhouse gases (GHGs) emitted by human activities, accounting for approximately 76% and 16% of global emissions, respectively. Current projections based on existing policies suggest that net GHG emissions in the European Union could be reduced by about 47% by 2030 compared with 1990 levels, while additional planned measures may increase this reduction to around 54%. Nevertheless, achieving climate neutrality by 2050 will require further substantial efforts from EU Member States (European Environmental Agency, 2025).

Although methane is widely recognized as a major GHG, it also serves as an important feedstock in chemical and energy-related applications, largely because of its high hydrogen content relative to carbon. In response to the increasing demand for cleaner and hydrogen-oriented energy technologies, significant efforts have been directed toward developing improved methane conversion pathways. Steam methane reforming (SMR, Eq. 1) remains the most established industrial method for syngas generation. However, other processes, including dry reforming (DRM), methane pyrolysis (MP), and partial oxidation (POM), are being increasingly explored as alternative solutions.

$$CH_4 + H_2O \rightleftharpoons CO + 3H_2, \quad \Delta H_r = 205.9 \left[\frac{kJ}{mol}\right] \quad (1)$$

DRM (Eq. 2) offers an environmentally friendly route by consuming CO_2 and CH_4 to produce an equimolar mixture of H_2 and CO, suitable for Fischer-Tropsch synthesis (Taherian et al., 2017), long-chain hydrocarbons, oxo-alcohols (Gadalla and Bower, 1988), and dimethyl ether (DME). MP (Eq. 3) generates H_2 without CO_2 emissions, producing solid carbon as a valuable byproduct for industrial applications, making it a bridge technology toward renewable fuels (Sánchez-Bastardo et al., 2021). POM (Eq. 4) is exothermic and energy-efficient but requires pure oxygen, posing challenges such as hot-spot formation, catalyst sintering, and higher capital costs.

$$CH_4 + CO_2 \rightleftharpoons 2H_2 + 2CO, \quad \Delta H_r = 247.0 \left[\frac{kJ}{mol}\right] \quad (2)$$

$$CH_4 \rightleftharpoons C_{(s)} + 2H_2, \quad \Delta H_r = 75.0 \left[\frac{kJ}{mol}\right] \quad (3)$$

$$CH_4 + 0.5O_2 \rightleftharpoons CO + 2H_2, \quad \Delta H_r = -36.0 \left[\frac{kJ}{mol}\right] \quad (4)$$

Overall, CH_4 conversion processes are inherently complex, involving multiple simultaneous reactions as well as coupled heat, mass, and momentum transfer phenomena. Consequently, their mathematical modelling is challenging, requiring the integration of detailed kinetic mechanisms, reactor hydrodynamics, and thermodynamic constraints.

Thermodynamics, in particular, plays an important role in determining the equilibrium compositions of gas and solid phases,

© 2026. The Author(s). This is an open-access article distributed under the terms of the Creative Commons Attribution (CC-BY 4.0, https://creativecommons.org/licenses/by/4.0/), which permits unrestricted use, distribution, and reproduction in any medium, provided the original author and source are credited.

which is essential for process design, optimization, and identifying the fundamental thermodynamic limits of CH_4 conversion. Reaction kinetics, especially when detailed mechanisms are involved, is also highly demanding. Accurate modelling requires the determination of rate constants and activation energies for multiple elementary reactions, as well as careful consideration of adsorption, surface reactions, activation processes, intermediate species, and catalyst behaviour.

Additionally, kinetic models usually need to be coupled with transport phenomena, accounting for heat and mass transfer to accurately predict reactor performance under real operating conditions. Often, multiscale modelling is necessary to integrate molecular-level reaction information with reactor-scale hydrodynamics.

To the best of our knowledge, no studies have provided a comprehensive overview of ANN applications in hydrogen and syngas production from methane via thermochemical conversion. This work aims to fill that gap.

2. ARTIFICIAL NEURAL NETWORKS

To overcome the abovementioned challenges, various machine learning (ML) techniques have been applied. In particular, ANNs constitute a class of parametric nonlinear models widely used in supervised learning tasks that require approximation of complex input-output relationships (Cybenko, 1989; Hornik et al., 1989). ML methods are generally categorized into supervised, unsupervised, semi-supervised and reinforcement learning, however, supervised approaches are of primary relevance in this work because they enable predictive modelling from labelled datasets. Common supervised techniques include regression models, classification algorithms such as decision trees and support vector machines, ensemble learning methods and ANN architectures including convolutional and recurrent neural networks. It is also worth noting that recent developments in physics-informed neural networks (PINNs) offer a promising hybrid approach by embedding thermodynamic or kinetic constraints into machine-learning models. Such methods may improve interpretability, reduce data requirements, and enhance predictive robustness, particularly for complex chemical process systems.

In the feedforward ANN architecture considered here in more detail, neuron outputs are computed as weighted transformations of inputs followed by nonlinear activation functions. For a multilayer perceptron (MLP) with a single hidden layer, the network output can be expressed as

$$\begin{aligned}\text{outputs} = y_k &= \sigma_2\left(\sum_{i=0}^{K} w_{ki}^{e} v_i\right) \\ &= \sigma_2\left(\sum_{i=0}^{K} w_{ki}^{e}\sigma_1\left(\sum_{j=0}^{N} w_{ij}^{h} x_j\right)\right)\end{aligned} \tag{5}$$

where: x_j is the *j-th* input signal, w_{ij}^{h} are weights connecting the input layer to hidden neurons, w_{ki}^{e} are weights connecting hidden neurons to outputs, v_i represents hidden layer activations, σ_1 and σ_2 are activation functions (Eqs. 6–7). A schematic representation of this architecture is shown on the left in Figure 1.

The hidden layer may employ, for example, the bipolar sigmoidal activation function (Alsaffar et al., 2020; Cherbański et al., 2026a)

$$\sigma_1(S) = \tanh(S) \tag{6}$$

which introduces nonlinearity while keeping differentiability required for gradient-based optimization. The output layer uses a linear activation

$$\sigma_2(S) = S \tag{7}$$

Network parameters are estimated by minimizing a loss function, typically the mean squared error (MSE):

$$E = E\left(\vec{w}\right) = \frac{1}{P}\sum_{p=1}^{P}\sum_{k=1}^{M}\left(y_k^{(p)} - d_k^{(p)}\right)^2 \tag{8}$$

where P denotes the number of samples, M is the number of output neurons, $y_k^{(p)}$ is the network prediction, and $d_k^{(p)}$ is the corresponding target value. Optimization is generally performed using backpropagation combined with gradient-based algorithms.

Apart from MLPs, another class of feedforward ANNs, called Radial Basis Function (RBF) networks, is also often used (Figure 1). RBF networks employ a nonlinear transformation of the input data by introducing a layer of hidden neurons based on a radially varying function centred around a priori selected centres. The output of the hidden layer is calculated using the following expression:

$$v_i = \sigma_1\left(\left\|\vec{x} - \vec{c}_i\right\|\right) \tag{9}$$

where $\left\|\vec{x} - \vec{c}_i\right\|$ means the distance between input vector data $\vec{x}$ and centroid vector $\vec{c}_i$ estimated by k-mean algorithm (unsupervised learning method), σ_1 is the similarity function (kind of radial basis function), often defined as Gaussian density probability function

$$\sigma_1(S) = \frac{1}{s\sqrt{2\pi}} e^{-\frac{(S-\mu)^2}{2s^2}} \tag{10}$$

where $S \equiv \left\|\vec{x} - \vec{c}_i\right\|$, μ is the mean input vector, s represents its standard deviation. The output layer is described by (7) and the output is given by

$$\begin{aligned}\text{outputs} = y_k &= \sigma_2\left(\sum_{i=0}^{K} w_{ki}^{e} v_i\right) \\ &= \sigma_2\left(\sum_{i=0}^{K} w_{ki}^{e}\sigma_1\left(\left\|\vec{x} - \vec{c}_i\right\|\right)\right)\end{aligned} \tag{11}$$

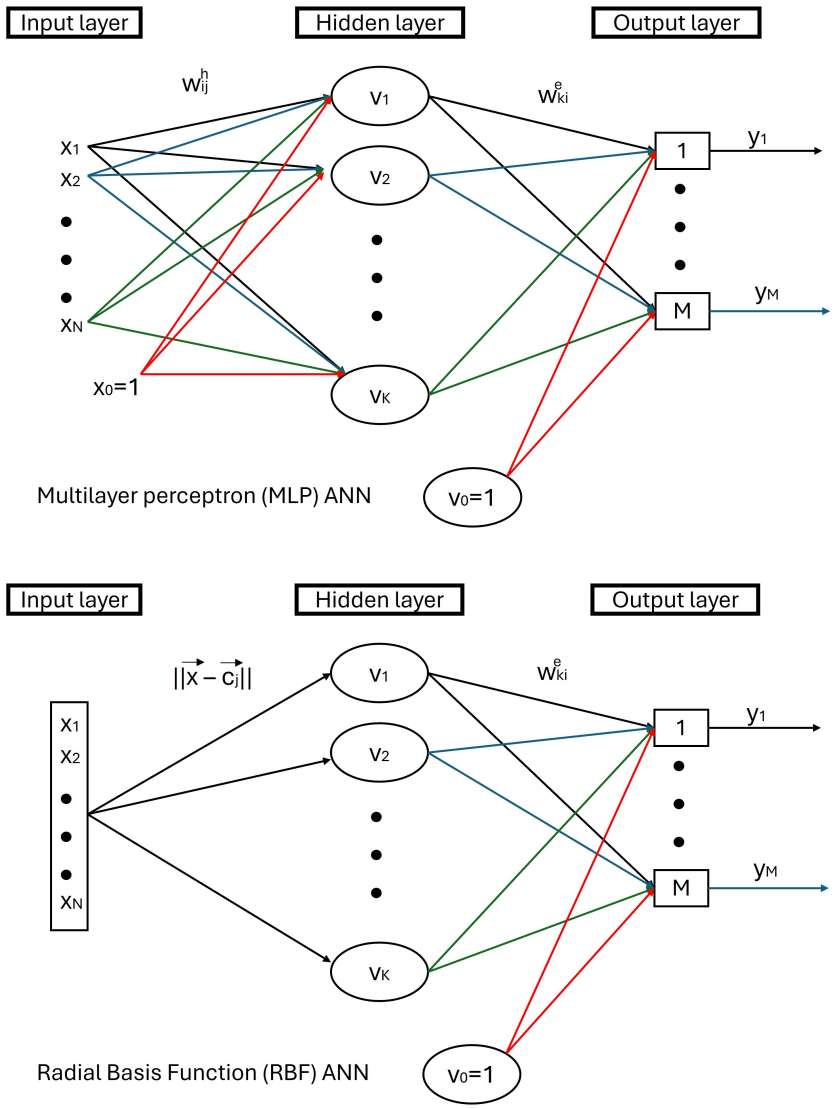

Figure 1. Structures of MLP (left) and RBF (right) ANNs.

RBF networks offer several advantages over MLPs, particularly in their ability to model nonlinear functions using a single hidden layer, whereas MLPs often require more complex architectures. In addition, RBF networks can be trained significantly faster than MLPs and may achieve higher accuracy for localized, well-clustered datasets. However, their performance tends to deteriorate when the data are sparse, scattered, or when the training set is limited in size.

From a theoretical perspective, the approximation capability of both RBF and MLP networks is supported by the universal approximation theorem (Cybenko, 1989; Hornik et al., 1989), which states that feedforward neural networks with at least one hidden layer and a non-polynomial activation function can approximate any continuous function on a compact domain to arbitrary accuracy, provided a sufficient number of hidden units is available.

Despite this strong theoretical foundation, the practical performance of ANNs depends critically on the quality and representativeness of the training data. In particular, while ANNs can interpolate complex nonlinear relationships effectively, their ability to extrapolate beyond the range of the training data is limited and may lead to unreliable predictions.

ML model performance is frequently evaluated using k-fold cross-validation (CV), a robust technique that utilizes the entire dataset to provide a reliable estimate of model generalization. This method is particularly effective at mitigating the risk of overfitting, a common challenge in training ANNs. The procedure involves splitting the dataset into k equal-sized subsets (i.e. folds). The model is then trained and validated in k iterations; in each cycle, $k-1$ folds are used for model training, while the remaining fold is used for validation. The choice of the parameter k depends on the size and nature of the dataset. For large datasets, a lower value, such as $k=3$, is often selected to minimize computational costs and the number of training iterations. For small datasets, larger values of k are typically preferred to ensure that the model is trained on a sufficiently large portion of the data

in each iteration. The strategy used for the data splitting is of equal importance, especially if the samples are sorted by class within the original dataset. To optimize the effectiveness of the method, stratification should be employed. This technique ensures that the proportion of individual classes in each validation fold remains approximately consistent with the distribution in the entire training set.

Network performance is frequently checked using the following parameters:

- Root Mean Squared Error (RMSE)

$$\mathrm{RMSE} = \sqrt{\frac{1}{PM}\sum_{p=1}^{P}\sum_{i=1}^{M}\left(y_i^{(p)} - d_i^{(p)}\right)^2} \tag{12}$$

- Mean Absolute Error (MAE)

$$\mathrm{MAE} = \frac{1}{PM}\sum_{p=1}^{P}\sum_{i=1}^{M}\left|y_i^{(p)} - d_i^{(p)}\right| \tag{13}$$

- Determination coefficient $\boldsymbol{R^2}$

$$R^2 = 1 - \frac{\sum_{p=1}^{P}\sum_{i=1}^{M}\left(y_i^{(p)} - d_i^{(p)}\right)^2}{\sum_{p=1}^{P}\sum_{i=1}^{M}\left(d_i^{(p)} - \overline{d}\right)^2} \tag{14}$$

where the mean value of destination is defined as follows

$$\overline{d} = \frac{1}{PM}\sum_{p=1}^{P}\sum_{i=1}^{M} d_i^{(p)} \tag{15}$$

- Standard Error of the Estimate (SEE)

$$\mathrm{SEE} = \sqrt{\frac{1}{(P-k)M}\sum_{p=1}^{P}\sum_{i=1}^{M}\left(y_i^{(p)} - d_i^{(p)}\right)^2} \tag{16}$$

where k is the number of estimated parameters.

- t-Student test a parametric statistical test used to compare the means of two groups (calculated output value and destination) to see whether the differences are statistically significant or due to chance.

Throughout this article, the terms *small* and *large* dataset are used. In the context of this work small datasets refer to studies containing fewer than approximately 100–200 samples, which is typical for experimental kinetic investigations with limited measurements (e.g. 27–75 patterns in several DRM studies in Table 3), while large datasets refer to datasets exceeding 1000 samples, typically derived from extensive literature databases, simulations or industrial-scale modelling (e.g. 2200+ samples in thermodynamic and process modelling studies in Table 3 and Table 4).

3. THERMODYNAMICS AND REACTION KINETICS

3.1. ANN of thermodynamic equilibrium modelling

Several studies have investigated the thermodynamic equilibrium for SMR (Ahmad et al., 2022; Ahmad et al., 2025; Demidov et al., 2011; Di Nardo et al., 2024; Jabbour, 2020), DRM (Ahmad et al., 2022; Ahmad et al., 2025; Demidov et al., 2011; Jabbour, 2020; Jensen and Duyar, 2021), POM (Ahmad et al., 2022; Ahmad et al., 2025; Zhu et al., 2001) and MP (Ahmad et al., 2022; Ahmad et al., 2025; Guéret et al., 1997) using the conventional Gibbs free energy minimization approach. In addition, equilibrium analyses have been extended to steam reforming of liquid fuels such as methanol (Di Nardo et al., 2024; Faungnawakij et al., 2006), ethanol (Di Nardo et al., 2024; Lima da Silva et al., 2009; Rossi et al., 2009), glycerol (Adhikari et al., 2007; Di Nardo et al., 2024; Ismaila et al., 2021; Rossi et al., 2009), as well as coal gasification (Ahmad et al., 2025; Shabbar and Janajreh, 2013).

While the Gibbs minimization method is well established and widely applied, data-driven approaches may offer advantages, particularly when rapid predictions or integration of equilibrium calculations into CFD simulations is required. Although ANNs have been successfully employed for modelling liquid-liquid and vapour-liquid equilibria (Carranza-Abaid et al., 2023; Del-Mazo-Alvarado and Bonilla-Petriciolet, 2022; Nguyen et al., 2007; Piotrowski et al., 2003; Reynel-Ávila et al., 2019), their application to equilibrium prediction in CH_4-based thermochemical conversion processes remains limited. For example, ANNs were used to model the steam reforming of naphthalene, using datasets generated from thermodynamic equilibrium calculations (Igwegbe et al., 2021). The models accurately captured the effects of temperature and steam-to-oil ratio on product selectivity, yielding R^2 values above 0.99 and RMSE values below 1 mol% for all datasets.

To address this gap, ANNs were applied to predict equilibrium gas composition and carbon formation in MP and various reforming processes (Cherbański et al., 2026a). In that study, equilibrium compositions for MP, DRM, SMR and POM were first calculated using Gibbs free energy minimization. The analysis considered the principal gaseous species (CH_4, CO_2, H_2, CO, H_2O, O_2 and N_2), as well as solid carbon, enabling the prediction of gas-phase compositions together with the equilibrium amount of solid carbon formed. Non-ideal gas behaviour was accounted for using the Peng-Robinson equation of state, while thermodynamic properties were obtained from standard databases and literature correlations. The minimization was performed subject to elemental mass balance constraints and non-negativity of species amounts. Model predictions were validated against literature equilibrium data for MP, showing very good agreement over a range of temperatures and pressures.

ANNs were then employed as data-driven models to predict equilibrium gas compositions and carbon yield in the above-mentioned processes. The input variables included feed composition expressed as molar ratios (CO_2/CH_4, H_2O/CH_4, O_2/CH_4), temperature, and pressure, which together define the thermodynamic state of the system (Table 1). The outputs comprised the mole fractions of the main gaseous species (CH_4, CO_2, CO, H_2, H_2O) and the carbon yield, enabling simultaneous assessment of gas-phase composition and carbon formation.

A feedforward ANN with a single hidden layer was adopted in the computations, as such architectures are generally sufficient to approximate nonlinear thermodynamic relationships while maintaining model simplicity. The network was trained using datasets generated from Gibbs free energy minimization calculations across a wide range of operating conditions. Separate validation and testing datasets were used to assess predictive accuracy and minimize overfitting.

The ANN predictions generally showed excellent agreement with equilibrium calculations, particularly for gaseous species, although slightly lower accuracy was observed for carbon yield, likely due to its stronger sensitivity to process conditions (Figure 2).

Compared with simpler data-driven approaches such as third-, fourth-, and fifth-order polynomials, ANNs provided superior predictive performance while retaining significantly lower computational cost than full thermodynamic calculations. This confirms that ANNs can be readily integrated into process optimization and control frameworks, where rapid prediction of equilibrium compositions enables dynamic adjustment of operating parameters. However, their reliability depends on the quality and representativeness of the training data, and extrapolation beyond the training domain remains a limitation.

3.2. ANN modelling of reaction kinetics

Several studies have demonstrated the effectiveness of ANNs in modelling and predicting reaction kinetics in various methane reforming processes. For example, the complex kinetics of tri-reforming of methane (TRM), integrating DRM, SMR, and POM, were investigated (de Souza et al., 2025). The developed ANN model accurately predicted CH_4 conversion across a wide range of experimental conditions, identifying reaction temperature as the most influential operational parameter. Analysis of the complete dataset showed that operational variables accounted for 68.5% of the total relative importance, with temperature being the dominant factor, whereas catalyst preparation variables contributed 31.5%. The model was trained using 6,700 experimental data points collected from the literature, involving Ni-based catalysts. Input variables included Ni content (wt.%), reaction temperature, and feed molar ratios (CO_2/CH_4, H_2O/CH_4, and O_2/CH_4), while CH_4 conversion served as the output variable. The network architecture, training strategy, and performance metrics are summarized in Table 3. Model validation using previously unseen data demonstrated strong predictive capability and generalization. The reported RMSE values for DRM, SRM, POM, and the combined TRM process were 3.44%, 2.20%, 1.61%, and 4.48%, respectively, confirming the robustness of the approach. Importantly, the study demonstrated that datasets from individual reforming reactions can be integrated to evaluate the overall TRM process, thereby facilitating catalyst formulation and targeted material screening.

The application of ANNs was explored for modelling syngas production from DRM over a $Ni/CaFe_2O_4$ catalyst (Hossain et al., 2016). The MLP and RBF network architectures were employed to model experimental data. The ANN models were

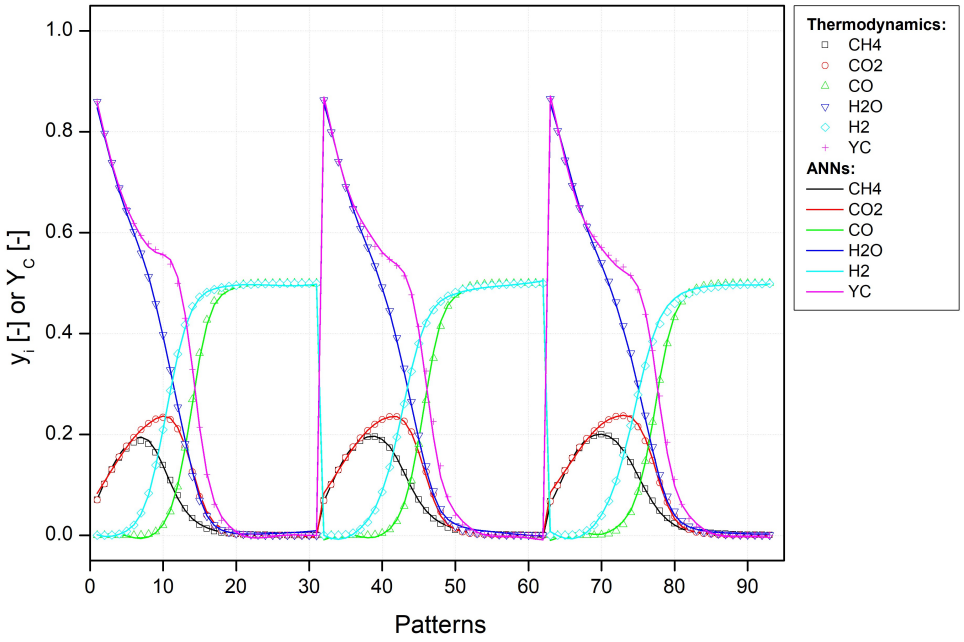

Figure 2. Comparison of the ANN predictions and targets for testing set No. 2.2 (see Table 1) (Cherbański et al., 2026a).

Table 1. List of training and test sets. Bold font indicates the interpolated domain (Cherbański et al., 2026a).

No	Training/ Testing	$\frac{n_{CO2}}{n_{CH4}}$	$\frac{n_{H2O}}{n_{CH4}}$	$\frac{n_{O2}}{n_{CH4}}$	T [°C]	P [bar]
1.	Training	0 (MP)	0	0	[0, 50, 100, . . . , 1500]	[1, 3, 5]
		0.25 (DRM)	0	0		
		0.5 (DRM)	0	0		
		0.75 (DRM)	0	0		
		1 (DRM)	0	0		
		1.25 (DRM)	0	0		
		1.5 (DRM)	0	0		
		1.75 (DRM)	0	0		
		2 (DRM)	0	0		
		0	0.25 (SMR)	0		
		0	0.5 (SMR)	0		
		0	0.75 (SMR)	0		
		0	1 (SMR)	0		
		0	1.25 (SMR)	0		
		0	1.5 (SMR)	0		
		0	1.75 (SMR)	0		
		0	2 (SMR)	0		
		0	0	0.1 (POM)		
		0	0	0.2 (POM)		
		0	0	0.3 (POM)		
		0	0	0.4 (POM)		
		0	0	0.5 (POM)		
		0	0	0.6 (POM)		
		0	0	0.7 (POM)		
2.1	Testing – interpolation	0 (MP)	0	0	[**25**, **75**, **125**, . . . , **1500**]	[1, 3, 5]
2.2		1 (DRM)	0	0		
2.3		0	1 (SMR)	0		
2.4		0	0	0.5 (POM)		
3.1	Testing – interpolation	0 (MP)	0	0	[0, 50, 100, . . . , 1500]	[**2**, **4**]
3.2		1 (DRM)	0	0		
3.3		0	1 (SMR)	0		
3.4		0	0	0.5 (POM)		
4.1	Testing – interpolation	**0.875 (DRM)**	0	0	[0, 50, 100, . . . , 1500]	[1, 3, 5]
4.2		0	**1.125 (SMR)**	0		
4.3		**0**	**0**	**0.45 (POM)**		
5.1	Testing – interpolation	**0.875 (DRM)**	0	0	[**25**, **75**, **125**, . . . , **1500**]	[**2**, **4**]
5.2		0	**1.125 (SMR)**	0		
5.3		0	0	**0.45 (POM)**		

developed using catalyst metal loading (5–15 wt.%), feed molar ratio (0.4–1.0), and reaction temperature as input variables, while the H_2 and CO yields as well as the CH_4 and CO_2 conversions were defined as output parameters. The predictive capabilities of the MLP- and RBF-based models were statistically evaluated and compared. The MLP model demonstrated superior performance, achieving higher coefficients of determination. The statistical analysis was also performed using a *t*-test on the predicted outputs, where the *t*-statistic quantified the difference between predicted and experimental mean values relative to data variability, and the resulting low *p*-values ($p < 0.005$) indicated that these differences were not due to random variation. This confirmed the higher predictive accuracy and statistical significance of the MLP model relative to the RBF approach. Overall, their findings indicated that the MLP architecture provided a more reliable tool for modelling syngas production from DRM over a $Ni/CaFe_2O_4$ catalyst, supporting its applicability in catalyst performance evaluation and process optimization.

Syngas production via DRM over a ceria-supported cobalt catalyst was investigated using a hybrid experimental-modelling approach combining ANNs with a Box-Behnken design (Ayodele and Cheng, 2015). Experimental data obtained from a fixed-bed reactor were used to evaluate the effects of reaction temperature, CH_4 partial pressure, and reactant feed ratio on CH_4 and CO_2 conversions. The ANN model was trained to capture the nonlinear relationships between operating variables and conversions, showing good agreement between predicted and experimental results. Integration of ANN with response surface methodology enabled process optimization, identifying optimal conditions at 728 °C, a CH_4 partial pressure of 46.85 kPa, and a feed ratio of 0.60, corresponding to CH_4 and CO_2 conversions of 74.84% and 76.49%, respectively. The study demonstrated that data-driven models can effectively support optimization of dry reforming systems without relying on detailed mechanistic kinetic formulations.

ANNs were further applied to model the kinetics of CO-rich hydrogen production during DRM over a Co/Pr_2O_3 catalyst (Ayodele et al., 2019). Experimental data obtained from 50 runs designed using a central composite experimental design were used to train the neural network. Reaction temperature as well as the partial pressures of CH_4 and CO_2 were considered as input variables, while the production rates of H_2 and CO were defined as the network outputs. A feedforward MLP architecture with a single hidden layer was implemented, and several training algorithms were evaluated, including the Levenberg-Marquardt, Bayesian regularization, and scaled conjugate gradient methods. The optimal network architectures were determined by minimizing MSE for hidden layers containing between 1 and 20 neurons. The developed ANN models demonstrated high predictive accuracy, with coefficients of determination exceeding 0.9 and strong correlation between predicted and experimental production rates. Among the evaluated training approaches, Bayesian regularization provided the best overall performance, yielding the lowest prediction error and improved model generalization. The study confirmed that ANN-based models can effectively capture the nonlinear relationships between reaction conditions and syngas production rates in DRM systems, providing a practical computational tool for analysing catalytic performance and supporting process optimization.

ANNs were employed to calibrate and improve the reliability of a kinetic model describing the steam reforming of naphtha compounds (hexane and heptane) over a NiMgAl catalyst synthesized from hydrotalcite-derived precursors (Morlanés et al., 2022). Multiple approaches were explored to identify the most accurate kinetic representation and to evaluate its robustness. The developed models incorporate key reactions such as hydrocarbon steam reforming, the water-gas shift reaction, and methanation. The model was validated across a broad spectrum of operating conditions using both simplified and real feedstocks, including methane, naphtha, diesel, and vegetable oil. The results demonstrate the effectiveness of ANNs in analysing complex reaction networks. Furthermore, the proposed kinetic framework can serve as a valuable tool for simulating process strategies and supporting the scale-up of reforming systems for hydrogen production.

Response Surface Methodology (RSM) and Radial Basis Function Neural Network (RBFNN) were employed to investigate and optimize the molecular dynamics of DRM over a novel Ni–Sr–Zr–Al (5Ni+3Sr/10Zr+Al) catalyst (Gendy et al., 2024). To assess how key operating parameters, namely hourly space velocity, reaction temperature, and the CO_2/CH_4 molar ratio, affect conversion efficiency and product distribution, optimal process conditions were predicted. In this context, ANN significantly outperformed RSM in terms of predictive accuracy.

3.3. ANN modelling of catalyst deactivation by coking

Predicting catalyst coking under varying operational conditions remains a significant challenge in various CH_4 conversion processes. The complex interplay of factors influencing coking mechanisms makes conventional modelling approaches inadequate. To overcome this, ANNs have emerged as powerful computational tools for forecasting catalyst performance, including coking behaviour, by learning nonlinear relationships from experimental data.

Data-driven approaches for catalyst coking are still relatively rare. Most studies focus on predicting the effect of operating conditions on the final mass of carbon deposits. For example, a full factorial experimental design was employed to systematize and evaluate the effects of the CH_4/CO_2 molar ratio, reaction temperature, and N_2 flow rate on carbon deposition (Alsaffar et al., 2020). Experimental data from 170 runs were used to develop and compare two ANN architectures: MLP and RBF. Both models were trained to predict carbon deposition per gram of catalyst. Optimization of the hidden layer

resulted in 16 and 20 neurons for the MLP and RBF models, corresponding to network architectures of 3-16-1 and 3-20-1, respectively. Statistical analysis demonstrated that the RBF provided superior predictive performance under both above- and below-stoichiometric conditions. For the MLP model, MSE values of 0.048 and 0.00285 were obtained, with corresponding R^2 values of 0.945 and 0.965. In contrast, the RBF achieved lower MSE values of 0.0073 and 0.00015, with R^2 values of 0.987 in both cases, indicating improved accuracy and robustness. Based on these results, the RBF was identified as the more reliable predictor of carbon deposition during hydrogen-rich syngas production via DRM. Furthermore, analysis of input variable importance revealed that the dominant factor influencing carbon deposition depended on the stoichiometric regime: reaction temperature was the most influential parameter under above-stoichiometric conditions, whereas the CH_4/CO_2 ratio had the greatest impact under below-stoichiometric conditions.

Both MLP and RBF ANN models were developed to predict carbon deposition during DRM under varying temperatures, N_2 flow rates, and CH_4/CO_2 molar ratios (Fang et al., 2025). The results indicated that the RBF network outperformed the MLP model in terms of predictive accuracy. To improve model reliability and reduce the risk of overfitting, k-fold cross-validation was applied for hyperparameter optimization and model selection. Their work has further highlighted the challenges associated with limited datasets, which are common in catalytic research due to experimental cost and time constraints. In one comparative study, MLP and RBF ANNs were evaluated across multiple random train-test splits to assess performance stability. The RBF architecture consistently demonstrated superior accuracy and robustness. To address the instability introduced by random data partitioning in small-sample regimes, a structured k-fold cross-validation framework was implemented, leading to the development of an optimized RBF model. The improved model achieved high predictive performance on unseen data (MSE = 0.0018, R^2 = 0.9882), with substantial reductions in prediction error and improved explanatory power relative to repeated random validations.

A more comprehensive approach to modelling catalyst deactivation was presented by Kumbhat et al. (2024), who developed ML models to predict the performance of Ni-based catalysts during both steam and dry reforming of biogas containing trace amounts of H_2S. In contrast to studies focusing solely on carbon deposition, this work addressed the combined effects of carbon formation and sulphur poisoning, which together govern catalyst deactivation under realistic reforming conditions. The authors compiled experimental datasets from several literature sources covering a wide range of operating parameters, including temperature, CH_4/CO_2 ratio, H_2O/CH_4 ratio, weight hourly space velocity, and H_2S concentration in the feed gas. In addition to operating variables, the models also incorporated catalyst properties such as BET surface area, pore volume, pore size, nickel loading, metal dispersion, and Ni crystal size. Two ML algorithms were evaluated: ANNs and random forests (RF). The models were trained to predict reactor outlet compositions and reactant conversions, including CH_4 and CO_2 conversions as well as mole fractions of H_2, CO, CH_4, and CO_2. The results demonstrated that the RF model provided superior predictive accuracy compared to the ANN, achieving a mean overall R^2 of 0.979 and significantly lower prediction errors. Furthermore, the trained RF model successfully captured transient catalyst deactivation behaviour associated with the introduction of H_2S in the feed stream and was able to generalize to new experimental conditions after limited fine-tuning using a small subset of additional data. These findings highlight the potential of ML techniques not only for predicting carbon deposition but also for modelling more complex catalyst deactivation mechanisms arising from multiple interacting processes during methane reforming.

There is growing interest in the use of Solid Oxide Fuel Cells (SOFCs) powered by hydrocarbon fuels. One of the main challenges in enhancing steam reforming processes is expanding the operational window while minimizing carbon deposition. Such improvements can be achieved through modifications to the design of conventional nickel-based catalysts. In this context, a two-layer feedforward ANN trained via the backpropagation algorithm was employed to capture the influence of process parameters on methane reforming over $LaNi_xAl_{1-x}O_3$ (x = 0.1–0.9) (Ciou et al., 2007). The developed ANN model successfully described the relationship between catalytic performance and the structural properties of the catalyst.

Syngas production via DRM over $La_{1-x}Ce_xNi_{1-y}Fe_yO_3$ (x, y = 0–0.4) perovskite catalysts has been investigated (Abedini et al., 2018). A set of catalysts with varying compositions was designed using a central composite design (CCD) approach and synthesized through a sol-gel auto-combustion method. An ANN was employed to establish the relationship between both preparation and operating parameters and the catalytic performance in the DRM process. The input variables included nickel and lanthanum molar fractions, calcination temperature, and reaction temperature, while methane conversion was treated as the output variable. The optimal ANN architecture consisted of nine neurons in the hidden layer, providing accurate predictions of methane conversion. Subsequently, a genetic algorithm (GA) was applied to identify the optimal catalyst preparation conditions aimed at maximizing methane conversion.

Recent work further demonstrates that ANNs can accurately forecast the time evolution of coking on Fe/C catalysts during MP (Cherbański et al., 2026b). Experimental data on catalyst coking evolution during MP were collected using TGA under high-purity CH_4 and N_2 flows. Measurements were conducted between 850–950 °C on ~10 mg samples of Fe/C catalyst (L'hospital et al., 2024; 2025). Each measurement included three stages: (i) heating under N_2, (ii) ramping to set temperature, and (iii) isothermal coking. Several experiments

at various temperatures were analysed, with baseline corrections applied. Thermograms of catalyst mass versus time were processed using spline interpolation with 15 s interval. The relative catalyst mass during coking was recalculated assuming 100% mass at the start of CH_4 exposure. ANNs of various architectures were trained on the thermogravimetric data to forecast coking behaviour. Input data were prepared using a sliding-window approach and normalized to $[0, 1]$ (Figure 3).

Feedforward networks with up to three hidden layers were evaluated using the Levenberg-Marquardt algorithm, with performance assessed by a weighted sum of squared errors across training, validation, and test datasets. Multi-step forecasting was performed by recursively feeding predicted outputs back into the input windows. MATLAB scripts automated preprocessing, windowing, and network training, exploring over 1,000 network architectures (Table 2).

Figure 4 shows the evolution of Fe/C catalyst coking during MP. As expected from Arrhenius-type behaviour, the coking rate increases with temperature. Note that minor deviations at the lowest temperatures after ∼25 minutes, which are likely due to experimental noise, were retained for ANN training to maintain realistic conditions.

Table 2. Tested ANN architectures and parameters for the sliding-window approach. The structure $x : y : z$ represents the initial number of neurons : the increment : the final number of neurons.

Window size	Number of nodes in the first hidden layer	Number of nodes in the second hidden layer	Number of nodes in the third hidden layer
2	1 : 1 : 10	1 : 1 : 10	0 : 1 : 10
3	1 : 1 : 10	1 : 1 : 10	0 : 1 : 10
5	1 : 1 : 15	1 : 1 : 15	0 : 1 : 15
7	1 : 1 : 15	1 : 1 : 15	0 : 1 : 15
10	1 : 1 : 25	1 : 1 : 15	0 : 1 : 15

Various feedforward ANN architectures were trained using sliding-window input data. Overall, selected networks demonstrated excellent performance across training, validation, and test datasets, accurately capturing the coking dynamics. Single-step forecasts closely matched experimental thermogravimetric profiles, highlighting the robustness and generalization capability of the ANNs. However, multi-step forecasting proved more challenging. Some architectures showed unstable predictions at lower temperatures, with small errors propagating and amplifying over time, causing oscillations

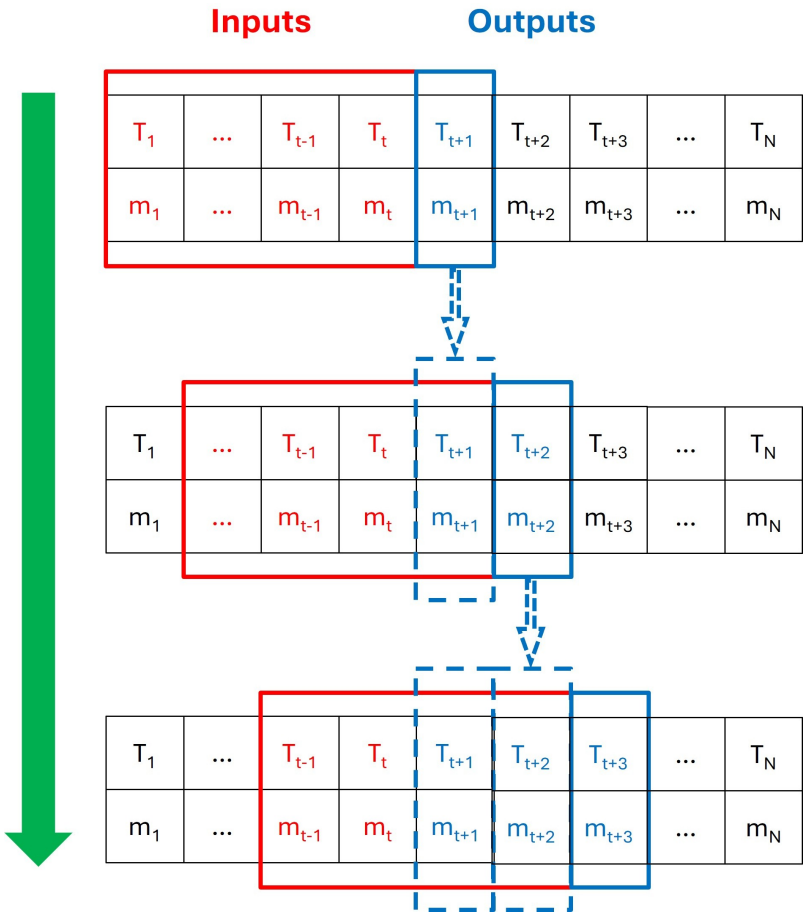

Figure 3. Illustration of a sliding window technique (solid lines) during preparation of training data (solid lines), and multi-step forecasting during predicting mode (solid and dashed lines) (Cherbański et al., 2026b).

around the experimental mass profiles. In contrast, ANN models trained with larger window sizes and optimized architectures produced reliable multi-step predictions across the full temperature range. For instance, an ANN with a window size of 10 and a 4-2-15 hidden layer structure accurately captured both training and test datasets (Figure 5), including

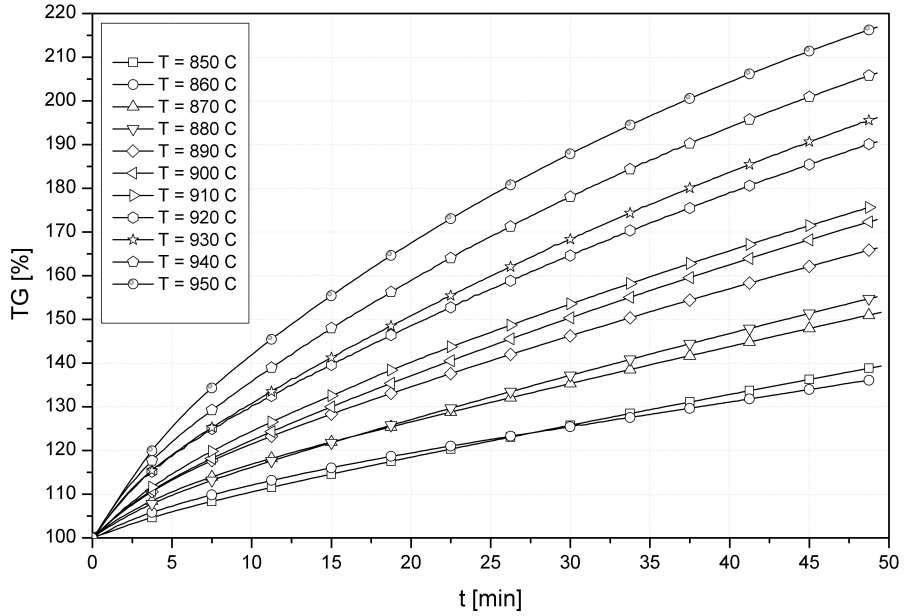

Figure 4. TGA of the Fe/C catalyst coking during methane pyrolysis at varying temperatures (Cherbański et al., 2026b).

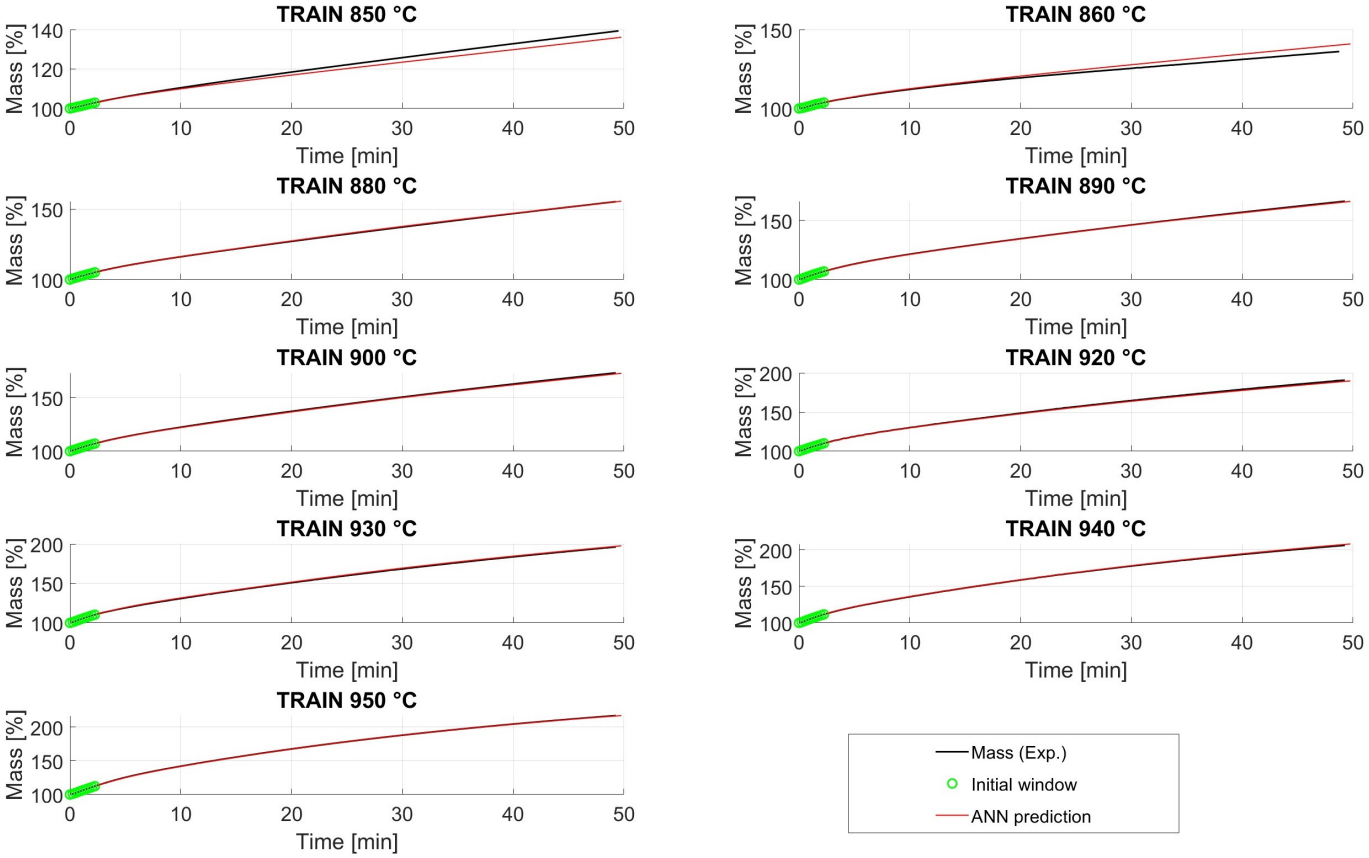

Figure 5. Results of the prediction phase using the training set: comparison between experimental relative mass profiles with those predicted by the ANN with a window size of 10 and a hidden layer structure of 4-2-15. The predictions start from the beginning (∼ 0 min) (Cherbański et al., 2026b).

temperatures not included in training, demonstrating strong generalization (Figure 6). Minor deviations at the lowest temperatures were attributed to experimental noise rather than model limitations.

These results indicate that ANN-based models can reliably forecast catalyst coking behaviour during MP, provided that appropriate network architectures and input preprocessing strategies are used. The study also highlights the importance of considering error propagation in multi-step forecasts and confirms that larger window sizes improve the stability and accuracy of long-term predictions.

The diversity of ANN approaches applied to thermodynamic and reaction kinetics modelling, including differences in data sources, network architectures and validation strategies, is summarized in Table 3.

4. REACTOR AND PROCESS PERFORMANCE MODELLING

ANNs have also been widely applied in reactor and process performance modelling. A summary of these studies, including industrial and simulation-based approaches, is presented in Table 4.

An ANN model was developed to predict the outlet gas composition in SMR (Pizoń et al., 2024a). The model was designed to estimate the molar fractions of H_2, CH_4, CO, and CO_2 as functions of five operational variables: reaction temperature, steam-to-methane ratio (H_2O/CH_4), nitrogen-to-methane ratio, inlet methane flow rate, and nickel catalyst mass. To overcome the limited availability of experimental data (72 original measurements), the authors implemented a weighted data augmentation strategy combining replicated experimental records, spline-interpolated data, and an extensive theoretical dataset generated from a kinetic model fitted via a GA.

The final training dataset consisted of 729 weighted experimental records, 305 interpolated records, and 9,441 theoretically generated samples. After normalization to the range $[0, 1]$, multiple ANN architectures were systematically evaluated. The optimal model comprised three hidden layers with a 6-8-6 neuron configuration and was trained using the BFGS Quasi-Newton backpropagation algorithm for 6,000 epochs. The selected architecture achieved a MSE of 0.00022, with a Pearson correlation coefficient of 0.97 and a Spearman correlation coefficient of 1.00, indicating excellent predictive performance.

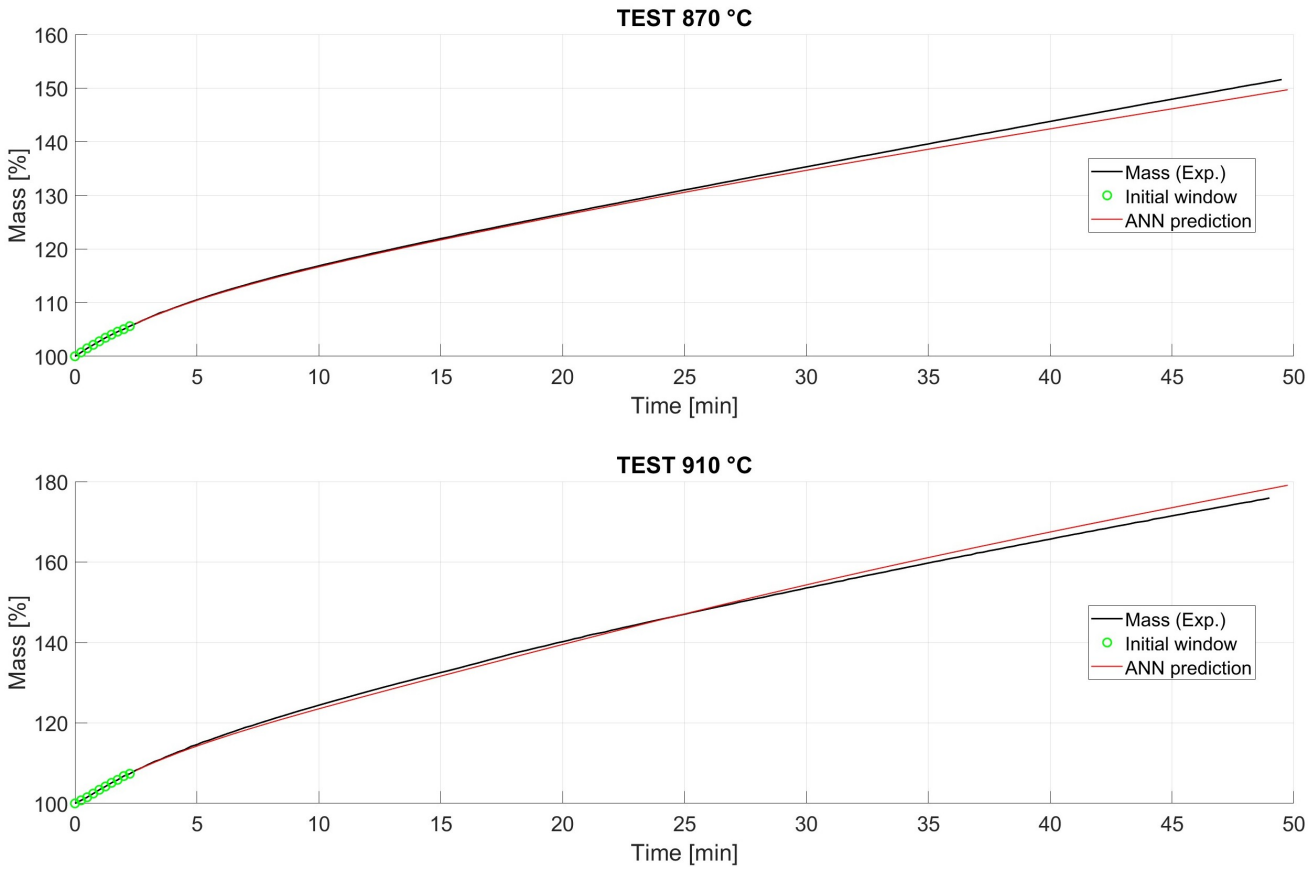

Figure 6. Results of the prediction phase using the test set: comparison between experimental relative mass profiles and those predicted by the ANN with a window size of 10 and a hidden layer structure of 4-2-15. The predictions start from the beginning (∼ 0 min) (Cherbański et al., 2026b).

Table 3. Summary of studies on ANN applications in thermodynamic and reaction kinetics modelling for hydrogen and syngas production from methane via thermochemical conversion.

Process	MP, DRM, SMR and POM (Cherbański et al., 2026a)	TRM (de Souza et al., 2025)	DRM (Hossain et al., 2016)	DRM (Ayodele and Cheng, 2015)	DRM (Ayodele et al., 2019)	DRM (Alsaffar et al., 2020)	DRM (Fang et al., 2025)
Domain	Thermodynamics	Kinetics	Kinetics	Kinetics	Kinetics	Kinetics (catalyst coking)	Kinetics (catalyst coking)
Data source (number of patterns)	Authors' calculation data (2,233)	Experimental data from literature (6,700)	Authors' experimental data (27)	Authors' experimental data (57)	Authors' experimental data obtained using central composite design (50)	Authors' experimental data (170)	Experimental data from literature (85)
Number and names of input variables	5: $\frac{CO_2}{CH_4}$, $\frac{H_2O}{CH_4}$, $\frac{O_2}{CH_4}$, T, P	5: Ni content, T, $\frac{CO_2}{CH_4}$, $\frac{H_2O}{CH_4}$, $\frac{O_2}{CH_4}$	3: metal loading, T, $\frac{CH_4}{CO_2}$	4: P_{CH4}, P_{CO2}, $\frac{CH_4}{CO_2}$, T	3: P_{CH4}, P_{CO2}, T	3: T, F_{N2}, $\frac{CH_4}{CO_2}$	3: T, F_{N2}, $\frac{CH_4}{CO_2}$
Number and names of output variable(s)	6: y_{CH4}, y_{CO2}, y_{CO}, y_{H2}, y_{H2O}, Y_C	1: X_{CH4}	4: X_{CH4}, X_{CO2}, Y_{H2}, Y_{CO}	4: r_{H2}, r_{CO}, X_{CH4}, X_{CO2}	2: r_{H2}, r_{CO}	1: C_{dep}	1: C_{dep}
Preprocessing data	Data normalization	NR	NR	NR	NR	RBF: data normalization; MLP: data standardization	NR
ANN architecture type	MLP	MLP	RBF and MLP	MLP	MLP	RBF and MLP	RBF and MLP
Best network architecture: inputs-hidden layers-outputs	5-40-6	5-4-1	RBF: 3-10-4; MLP: 3-12-4	4-16-4	RBF: 2-15-2-2; MLP: 2-13-2-2; SCG: 2-15-2-2	RBF: 3-20-1; MLP: 3-16-1	RBF: 3-max(65)-1; MLP: 3-5-1
Training	BP using LM	BP using Adam with BR and ES	RBF: not reported; MLP: BP	BP using LM	BP using LM, BR, SCG	RBF: LM; MLP: LM	RBF: NR; MLP: BP
Validation / Additional procedure	–	4-fold cross-validation	–	–	Model comparison between different training algorithms	–	5-fold cross-validation
Data split for training/ validation/ testing	70/15/15%	70/10/20%	70/15/15%	70/15/15%	70/15/15%	70/15/15%	76% (training, 5-fold CV)/ 24% (testing)
Network performance	MSE, R^2	MAE, RMSE, R^2	R^2, SEE, t-test	MSE, R^2, ARE	MSE, R^2	MSE, R	MSE, R^2

Table 3 continued

Process	Biogas SMR and DRM with H2S (Kumbhat et al., 2024)	MP (Cherbański et al., 2026b)	Steam reforming of model naphtha mixture (Morlanés et al., 2022)	DRM (Gendy et al., 2024)	SMR (SOFC) (Ciou et al., 2007)	DRM (Abedini et al., 2018)
Domain	Kinetics (catalyst deactivation: coking and sulphur poisoning)	Kinetics (catalyst coking)	Kinetics (model discrimination + kinetic modelling)	Kinetics (process optimization with RSM and ANN)	Kinetics (catalyst performance / process modelling in SOFC)	Kinetics (catalyst design and optimization using ANN + GA)
Data source (number of patterns)	Experimental data from literature ($\sim$ 300)	Authors' experimental data (2,200)	Authors' modelling and experimental data (1710 features per instance; 500 instances per model)	Authors' experimental data (28)	Authors' experimental data (not explicitly stated; generated via mass spectrometry)	Authors' experimental data (75)
Number and names of input variables	12: time, T, $\frac{CO_2}{CH_4}$, $\frac{H_2O}{CH_4}$, WHSV, c_{H2S}, BET surface area, pore size, pore volume, Ni content, Ni dispersion, Ni crystallite size	20: Sliding-window inputs (10 time steps $\times$ 2 variables: T and m_{cat})	Kinetic data (1710 features per instance: profiles of species vs. conditions – implicit inputs: T, $\frac{S}{C}$, $p_{naphtha}$, space time, compositions)	3: T, $\frac{CH_4}{CO_2}$, GHSV	6: T, time, lattice parameter, Ni molar ratio (in $LaNi_xAl_{1-x}O_3$), F_{CH4}, F_{H2O}	4: La mole fraction, Ni mole fraction, $T_{calcination}$, $T_{reaction}$
Number and names of output variable(s)	1: separate models for each output variable: X_{CH4}, X_{CO2}, y_{H2}, y_{CO}, y_{CH4}, y_{CO2}	2: T and m_{cat}	8-class classification (probability of kinetic model / rate law)	3: X_{CH4}, X_{CO2}, $\frac{H_2}{CO}$	3: F_{CH4}, F_{CO}, F_{H2O}	1: X_{CH4}
Preprocessing data	Data normalization and feature scaling	Data normalization	Data standardization (mean removal, unit variance), feature selection ($10\% < X < 90\%$)	Data normalization	Data normalization	Data normalization
ANN architecture type	MLP	MLP	MLP	RBF	MLP	MLP
Best network architecture: inputs-hidden layers-outputs	Separate ANNs for the output variables 12-24-1	20-4-2-15-2	1710-(50, 100, 200, 500)-8	3-10-1 (separate models for each output variable)	6-(optimized, not explicitly fixed)-3 (single hidden layer; number of neurons determined empirically)	4-9-1
Training	BP using Adam	BP using LM	Adam, categorical cross-entropy, ReLU + Softmax	RBFNN	BP, gradient descent (MSE minimization)	BP using LM with ES

Table 3 continued

Process	Biogas SMR and DRM with H2S (Kumbhat et al., 2024)	MP (Cherbański et al., 2026b)	Steam reforming of model naphtha mixture (Morlanés et al., 2022)	DRM (Gendy et al., 2024)	SMR (SOFC) (Ciou et al., 2007)	DRM (Abedini et al., 2018)
Validation/ Additional procedure	Model comparison with Random Forest	–	10-fold cross-validation + grid search (hyperparameter tuning)	Model comparison with RSM; performance evaluation via multiple statistical metrics (R^2, RMSE, error analysis)	CV	ES + integration with GA for optimization
Data split for training/ validation/ testing	80/20% train-test split	70/12/18%	80/20% train-validation split, CV	Not explicitly split (small dataset; full dataset used for model fitting and evaluation)	70/10/20%	70/15/15%
Network performance	RMSE, R^2	Own objective function based on SSE	Classification accuracy, confusion matrix	R^2, RMSE	MSE	R^2, ARD

Variables: C_{dep} – carbon deposition, F – flow rate, m – mass, P – pressure, r – reaction rate, T – temperature, X – conversion, y – mole fraction, Y – yield, WHSV – weight hourly space velocity; Algorithms/Training methods: Adam – adaptive moment estimation algorithm, BP – backpropagation, BR – Bayesian regularization, ES – early stopping, BFGS quasi-Newton BP – Broyden-Fletcher-Goldfarb-Shanno quasi-Newton backpropagation, GA – genetic algorithm, LM – Levenberg-Marquardt, SCG – scaled conjugate gradient; Neural network types: MLP – multilayer perceptron, RBF – radial basis function; Performance metrics/statistics: ARD – average relative deviation, ARE – average relative error, MAE – mean absolute error, MSE – mean squared error, RMSE – root mean squared error, R – Pearson correlation coefficient, R^2 – coefficient of determination, S – Spearman rank correlation coefficient, SEE – standard error of estimate, Accuracy – classification accuracy; Additional terms: CV – cross-validation, ReLU – rectified linear unit, Softmax – normalized exponential activation function, Categorical cross-entropy – loss function for classification, Feature scaling/standardization – data preprocessing to zero mean and unit variance; NR – not reported

Table 4. Summary of ANN approaches applied to reactor and process performance modelling.

Process	SMR (Arcotumapathy et al., 2012)	SMR (Zamaniyan et al., 2013)	SMR (Vo et al., 2019)	DRM (Rahman and Biswas, 2024)	SE-SMR (Nkulikiyinka et al., 2020)	SMR (Jafarizadeh et al., 2024)	SMR (Shahid et al., 2025)	SMR (Ba-Alawi et al., 2026)
Domain	Catalyst design (set A) and reactor operation (set B) optimization	Industrial hydrogen plant	Reactor performance	Catalyst performance	Process performance	Reactor performance	Reactor performance + waste heat recovery	Process performance
Data source (number of patterns)	Experimental data from literature (200)	Authors' modelling data (100)	Authors' modelling data (81)	Experimental data from literature (28)	Authors' simulation data (13,756)	Authors' modelling data (625)	Authors' experimental and simulation data (491)	Authors' simulation data (30,000)
Number and names of input variables	Set A – 14: Ni loading, support types, promoters, T, P, $\frac{S}{C}$, space time, time-on-stream, catalyst reduction temperature Set B – 14: Ni loading, support types, promoters, T, P, $\frac{S}{C}$, time-on-stream, catalyst reduction temperature	4: T, P, $\frac{S}{C}$, $\frac{CO_2}{CH_4}$	4: Reactor: F and T, $\frac{S}{C}$, Furnace: F	5: T, GHSV, surface area, pore volume, pore diameter	4: Reformer: T, P, $\frac{S}{C}$, CaO/C; Regenerator: T	4: F, $\frac{S}{C}$, heat flux, tube length	1-4 (depending on configuration): $\frac{CH_4}{H_2O}$, T, P, heat duty (for C-15)	8: Reformer: T, P, F_{CH4}, F_{H2O}; HT- and LT-WGS reactors: T_{HT}, T_{LT}, P, F_{H2O}
Number and names of output variable(s)	Both sets – 1: X_{CH4}	3: T, y_{H2}, y_{CO}	7: T, v, P, y_{CH4}, y_{CO2}, y_{H2}, y_{CO}	1: Y_{H2}	6: Reformer – X_{CH4}, y_{H2O}, y_{CO}, y_{H2}; Regenerator – y_{H2O}, y_{CO2}	7: X_{CH4}, X_{H2O}, production rates: H_2, CO_2, CO, wall temperature, product temperature	1: F_{H2}	3: UPC, NCE, EEF
Preprocessing data	Data normalization, principal component analysis (PCA); noise reduction	NR	Principal component analysis based on singular value decomposition	NR	Data randomization and normalization	Data normalization	NR	Data standardization

Table 4 continued

Process	SMR (Arcotumapathy et al., 2012)	SMR (Zamaniyan et al., 2013)	SMR (Vo et al., 2019)	DRM (Rahman and Biswas, 2024)	SE-SMR (Nkulikiyinka et al., 2020)	SMR (Jafarizadeh et al., 2024)	SMR (Shahid et al., 2025)	SMR (Ba-Alawi et al., 2026)
ANN architecture type	MLP	MLP	MLP	MLP	MLP	MLP	MLP	MLP
Best network architecture: inputs-hidden layers-outputs	Set A: in 3 hidden layers (Fibonacci-based opimization), total 83 neurons Set B: in 2 hidden layers (Fibanocci-based optimization), total 9 neurons	4-5-3	NR	LM: 5-10-1; SCG: 5-8-1	NR	4-32-16-8-8-7	4-(2-10 hidden layers, $\sim$ 10 neurons each)-1	8-64-32-16-8-6-3
Training	BP using LM with ES	BP	BP	BP using LM, SCG, BR	NR	BP using Adam	BP using LM	BP using Adam with ES (final training)
Validation/ Additional procedure	Multi-error evaluation, weighted optimal combination of ANN models	–	–	NR	–	10% validation split from training data	Testing of multiple input combinations (C-1 – C-15), hidden layers (2-10), 5-fold CV	Data normalization
Data split for training/ validation/ testing	75/12.5/12.5%	50/25/25%	72/28% train-testing split	>90% train / <10% test + validation	NR	80/(10)/20%	Variable splits (test ratios: 10%, 20%, 30%)	60/20/20%
Network performance	SSE, MSE, RMSE, MAE, MAPE	R^2	ARE	MSE, R^2	MSE, RMSE, R^2	MSE, MAE	MSE, R^2	MSE, MAE, R^2

Table 4 continued

Process	ATR (Soltanimehr et al., 2026)	SMR (Pizoń et al., 2024a)	SMR (Pizoń et al., 2024b)	SMR (Pizoń et al., 2025)	SMR (Biermann et al., 2025)*	Electrified SMR (Samris et al., 2025)	DRM (Roh et al., 2024)	Reforming processes (Yalcin et al., 2024)
Domain	Industrial auto-thermal reformer performance	Reactor performance	Reactor performance	Reactor performance	Reactor performance	Reactor performance	Kinetics (catalyst performance prediction using hybrid ANN-QNN model)	Process performance
Data source (number of patterns)	CHEMKIN-based data coupled with PFR simulations (1300)	Authors' experimental, interpolated, and calculated data (10,475)	Authors' experimental, interpolated, and calculated data (NR)	Authors' experimental, interpolated, and calculated data (NR)	Authors' modelling data (NR)	Authors' modelling data (1748)	Literature + in-house experimental data ($\sim$ 300)	Authors' simulation data (NR)
Number and names of input variables	8: y_{CH4}, y_{H2O}, y_{CO}, y_{H2}, y_{CO2}, T + 2 unspecified	5: T, $\frac{S}{C}$, $\frac{N}{C}$, m_{cat}, F_{CH4}	NR	5: T, $\frac{S}{C}$, $\frac{N}{C}$, m_{cat}, F_{CH4}	6: T, p_{CH4}, p_{CO2}, p_{H2O}, p_{CO}, p_{H2}	4: Porosity, F, y_{CH4}, y_{H2O}	$\sim$ 65 input features (catalyst composition, temperature, GHSV, gas composition, reduction conditions)	CH_4 reforming – T, P, $\frac{S}{M}$, $\frac{O_2}{M}$; 3: methanol reforming – T, $\frac{S}{methanol}$, $\frac{O_2}{methanol}$; 3: diesel reforming – T, $\frac{S}{diesel}$, $\frac{O_2}{diesel}$
Number and names of output variable(s)	6: y_{CH4}, y_{H2O}, y_{CO}, y_{H2}, y_{CO2}, T	4: y_{CH4}, y_{CO2}, y_{H2}, c_{CO}	4: y_{CH4}, y_{CO2}, y_{H2}, c_{CO}	4: y_{CH4}, y_{CO2}, y_{H2}, c_{CO}	5: $\dot{s}_{CH4}$, $\dot{s}_{CO2}$, $\dot{s}_{H2O}$, $\dot{s}_{CO}$, $\dot{s}_{H2}$ (source terms embedded in the reactor model)	2: y_{CO2}, y_{H2}	1: X_{CH4}	CH_4 reforming – Y_{H2}, y_{CO}, X_{CH4}; 2: methanol and diesel reforming – Y_{H2}, y_{CO}
Preprocessing data	NR	Data normalization and weighting	Data normalization and weighting	Data normalization and weighting	Data scaling	Data normalization, Z-score normalization, SMOTE	Dimensionality reduction via ANN layers	Data randomization and normalization
ANN architecture type	MLP	MLP	MLP	MLP	PENN	PINN	Hybrid QNN (ANN + parametrized quantum circuit, PQC)	CNN

Table 4 continued

Process	ATR (Soltanimehr et al., 2026)	SMR (Pizoń et al., 2024a)	SMR (Pizoń et al., 2024b)	SMR (Pizoń et al., 2025)	SMR (Biermann et al., 2025)*	Electrified SMR (Samris et al., 2025)	DRM (Roh et al., 2024)	Reforming processes (Yalcin et al., 2024)
Best network architecture: inputs-hidden layers-outputs	8-8-6 (number of hidden neurons not explicitly reported)	5-6-8-6-4	NR-6-8-6-4	5-15-5-15-9-8-11-4	6-60-60-60-5	4-256-256-ResBlock(256x2)-128-64-2	ANN: 65-32-16-8-4-1; Hybrid QNN: 65-32-16-4-PQC-1	CNN architecture (convolutional layers + fully connected layers)
Training	BR using LM	BP using BFGS quasi-Newton	BP using BFGS quasi-Newton	Adam + Bayesian optimization	LBFGS	Multi-phase training regimen (warm-up phase and physics-informed loss using Adam)	BP using Adam with ES	BP using Adam
Validation/ Additional procedure	–	–	–	Bayesian hyperparameter optimization	Comparison with reference microkinetic reactor model	–	30 repeated runs; ANN vs hybrid QNN comparison; validation on independent dataset	NR
Data split for training/ validation/ testing	70/15/15%	NR	NR	82.35/17.64/0.01%	25/25/50%	70/15/15%	70/14/16%	80/10/10%
Network performance	MSE, R^2, AARD	R, S	R, S	MSE, R, R^2	Agreement with mechanistic model	R^2, MAE	R^2, MAE, AE	R^2, MAPE, MAE, RMSE

Variables: T – temperature, P – pressure, v – velocity, X – conversion, Y – yield, y – mole fraction, c – concentration, F – molar flow rate, GHSV – Gas Hourly Space Velocity, m – mass, $\frac{S}{C}$ – steam-to-carbon ratio, $\frac{N}{C}$ – nitrogen-to-carbon ratio, $\frac{S}{M}$ – steam-to-methane ratio; Algorithms/Training methods: Adam – adaptive moment estimation, BP – backpropagation, BR – Bayesian regularization, BFGS quasi-Newton – Broyden-Fletcher-Goldfarb-Shanno quasi-Newton backpropagation, LBFGS – limited-memory Broyden-Fletcher-Goldfarb-Shanno, LM – Levenberg-Marquardt, SCG – scaled conjugate gradient, SMOTE – Synthetic Minority Over-sampling Technique, NSGA-II – non-dominated sorting genetic algorithm II; Neural network types: CNN – convolutional neural network, MLP – multilayer perceptron, PINN – physics-informed neural network, PENN – physics-enhanced neural network; Performance metrics/statistics: MAE – mean absolute error, MAPE – mean absolute percentage error, MSE – mean squared error, RMSE – root mean squared error, R – Pearson correlation coefficient, R^2 – coefficient of determination, S – Spearman rank correlation coefficient, AARD – average absolute relative deviation; Additional terms: CFD – computational fluid dynamics, PFR – plug flow reactor, CV – cross-validation, UPC – unit production cost, NCE – net CO2-equivalent emission, EEF – energy efficiency, SE-SMR – sorption-enhanced steam methane reforming; NR – not reported

*) Ref. (Biermann et al., 2025) employs a physics-enhanced neural network embedded within a mechanistic microkinetic reactor model rather than a standalone data-driven MLP surrogate.

Validation against independent experimental measurements and kinetic simulation data confirmed strong agreement across varying methane flow rates, catalyst masses, H_2O/CH_4 ratios, and temperatures. Minor deviations observed at elevated temperatures were attributed to the predominance of non-equilibrium data in the training set, which limited the model's ability to accurately reproduce equilibrium effects. Compared with a standalone kinetic model (MSE = 0.0032) and previously reported ANN and nonlinear response surface models, the proposed framework demonstrated superior predictive performance, demonstrating that hybrid dataset construction can significantly improve ANN-based reformer modelling.

This concept was further expanded in a subsequent study by the same authors (Pizoń et al., 2024b), which demonstrated that an ANN-based simulator can effectively model the SMR process, delivering accurate predictions based on key operating variables such as temperature, inlet gas composition, methane flow rate, and nickel catalyst mass. The training procedure incorporated experimental, interpolated, and theoretical datasets. Multiple neural network configurations were evaluated, leading to the selection of an optimal architecture with a 5-6-8-6-4 structure. The developed ANN model was then applied to predict the concentrations of components in the outlet stream as functions of varying reformer operating conditions. A comparison between the ANN predictions and validation data confirmed that the model provides a reliable and suitable representation of the studied process.

In another study by the same authors (Pizoń et al., 2025), an artificial neural network was developed to model the SMR process. Conventional models typically describe either kinetic or equilibrium regimes, which limits their broader applicability. To overcome this limitation, a unified ANN-based model capable of representing both regimes was proposed. The network was trained on a dataset comprising experimental, interpolated, and theoretical data, further enhanced using data augmentation techniques. Bayesian optimization was applied to determine the most suitable network architecture. The final model consisted of an input layer with five neurons corresponding to key operating parameters, followed by six hidden layers arranged in a 15-5-15-9-8-11 configuration, and an output layer with four neurons representing the dry gas composition of the post-reaction mixture (CH_4, H_2, CO, and CO_2). The developed ANN exhibited high predictive accuracy in estimating the composition of the outlet gas under varying operating conditions. The results indicate that the proposed model is both robust and reliable for the analysed SMR process, making it a valuable tool for reactor design and process optimization.

Similarly, a three-layer feedforward ANN was proposed to represent the performance of an industrial hydrogen production plant (Zamaniyan et al., 2013). The network predicted product temperature, pressure, and the mole fractions of H_2 and CO as functions of feed temperature, reformer pressure, steam-to-carbon ratio (S/C ratio), and CO_2/CH_4 ratio. Training data were generated from detailed process simulations covering a broad range of operating conditions. A tangent sigmoid activation function was employed in both hidden and output layers, and the network was trained using a gradient descent algorithm. The optimal number of hidden neurons was determined by minimizing the MSE. ANN predictions closely reproduced the simulation results, indicating that the network successfully captured the nonlinear behaviour of the integrated hydrogen production process. By representing all major process units within a unified framework, the approach reduced the need for complex code-based simulations and enabled computationally efficient performance analysis and process optimization within the investigated operating range.

Extending ANN-based modelling toward physically detailed reactor simulations, datasets generated using computational fluid dynamics (CFD) were utilized to train and optimize a reduced-order (surrogate) model for an industrial-scale SMR reactor (Jafarizadeh et al., 2024). The ANN predicted seven key performance indicators, including CH_4 and H_2O conversions, H_2, CO_2 and CO production rates, wall temperature, and gas outlet temperature, as functions of reformer length, feed flow rate, surface heat flux, and S/C ratio. Two-dimensional axisymmetric CFD simulations were employed to generate the training data, enabling the network to capture complex spatially resolved reactor behaviour. The optimized architecture consisted of four hidden layers with a 32-16-8-8 neuron configuration. High predictive accuracy was achieved ($R^2 > 0.98$ for all target variables), confirming the model's ability to reproduce nonlinear reactor dynamics. Coupling the trained ANN with a random search optimization algorithm yielded a computationally efficient framework for maximizing hydrogen yield while minimizing reformer dimensions, significantly reducing dependence on resource-intensive CFD simulations.

A hybrid modelling framework combining a rigorous dynamic model of a steam methane reformer with an ANN surrogate was proposed to enable rapid prediction of reactor performance (Vo et al., 2019). The mechanistic model consisted of coupled sub-models describing a multiscale catalytic reactor, reactor tube wall, and furnace, which were linked through heat transfer and transport phenomena to capture the detailed behaviour of the reforming system. The validated dynamic model was subsequently used to generate training data through deterministic and stochastic simulations covering variations in four key operating variables: the reactor inlet flow rate, reactor inlet temperature, S/C ratio, and the inlet flow rate on the furnace side. To reduce the dimensionality of the generated dataset, principal component analysis based on singular value decomposition was applied prior to ANN training. A feedforward backpropagation neural network was then trained using 81 simulation cases to map the relationship between the operating conditions and the predicted outputs at the reactor outlet, including temperature, velocity, pressure, and mole fractions of the major components. Validation against additional simulation cases showed excellent agreement between ANN predictions and the dynamic model results, with pre-

diction errors below 2% and an overall accuracy of 98.91%. Moreover, the ANN surrogate significantly reduced the computational time required for prediction from approximately 1200 s for the full dynamic simulation to about 2 s. These results demonstrate that integrating rigorous mechanistic modelling with ANN-based surrogate models provides an effective approach for real-time monitoring, process optimization, and design of industrial steam methane reformers while maintaining high predictive accuracy.

Further advancing hybrid modelling strategies, a physics-enhanced neural network (PENN) framework was introduced to accelerate microkinetics-based simulations of industrial packed-bed reactors (Biermann et al., 2025). The study addressed the high computational cost of detailed microkinetic models, which typically involve large reaction mechanisms and stiff differential equation systems that constrain their practical use in large-scale optimization studies. Rather than replacing mechanistic modelling with a purely data-driven surrogate, the authors embedded neural networks within the first-principles framework to approximate computationally demanding components of the microkinetic rate expressions. Training data were generated from accurate microkinetic simulations across a broad range of temperatures, pressures, and feed compositions representative of industrial reforming conditions. By incorporating physical constraints and thermodynamic consistency directly into the network architecture, the proposed method preserved mechanistic consistency while substantially reducing computational time. The PENN-based model exhibited strong agreement with the reference mechanistic model and demonstrated improved numerical stability and extrapolation capability compared to standard feedforward ANN surrogates. The study demonstrates that PENN models can effectively link detailed reaction kinetics with industrial-scale process simulation.

A physics-informed neural network (PINN) framework was proposed for modelling electrified SMR, integrating first-principles modelling directly into the neural network architecture (Samris et al., 2025). Unlike conventional black-box ANNs, the model incorporated mass and energy conservation constraints into the loss function, enabling physically consistent predictions across a wide operating range. The framework combined CFD simulations with deep learning, where a detailed CFD model accounting for reactor geometry, reaction kinetics, and coupled heat and mass transfer phenomena was first developed and validated. A PINN model was subsequently trained using a database generated from the CFD simulations. The network used operating parameters such as applied voltage, catalyst porosity, mass flow rate, and H_2O/CH_4 ratio as input variables, while predicting key process indicators including hydrogen production, CO_2 and CO emissions, and reactor wall temperature. The incorporation of physics-based constraints improved model accuracy and generalization compared to purely data-driven approaches. Validation against the CFD model demonstrated excellent agreement, while substantially reducing computational cost, highlighting the potential of PINN-based surrogates for rapid optimization and real-time monitoring of electrified hydrogen production systems.

An integrated artificial intelligence framework was developed for modelling and multi-objective optimization of an industrial autothermal reformer (ATR) comprising a combustion chamber and a catalytic bed (Soltanimehr et al., 2026). The combustion section was simulated in CHEMKIN using the detailed GRI-3.0 kinetic mechanism (325 elementary reactions and 53 species), while the catalytic zone was modelled as a one-dimensional heterogeneous plug-flow reactor based on the kinetic model (Xu and Froment, 1989). To overcome the lack of direct coupling between CHEMKIN and MATLAB during optimization, approximately 1,300 datasets were generated from the validated combustion simulations and used to train a MLP neural network. The trained ANN was subsequently integrated with a multi-objective NSGA-II genetic algorithm to simultaneously maximize methane conversion and hydrogen yield while minimizing net CO_2 production. The optimal operating conditions increased CH_4 conversion to 99.6% and suggested the possibility of net CO_2 consumption under specific regimes. By combining detailed kinetic combustion modelling with ANN-based modelling and evolutionary optimization, the study demonstrated a computationally efficient strategy for optimizing complex ATR systems.

ANNs were utilized to estimate hydrogen yield in SMR as a function of key operating variables, including methane and steam flow rates, reactor pressure, temperature, and heat duty (Shahid et al., 2025). The results highlight the potential of data-driven approaches for enhancing hydrogen production processes. From a practical perspective, such models can be integrated into real-time monitoring and control systems for industrial reformers, enabling improved process efficiency, reduced energy demand, and increased hydrogen output. Furthermore, combining these approaches with carbon capture and storage (CCS) technologies, as well as fostering collaboration between academia and industry, may accelerate progress toward more sustainable hydrogen production at scale. Future research may also explore the application of optimization techniques, such as genetic algorithms and gradient-based methods, to identify optimal operating conditions and further improve process performance.

A rule-based supervisory multi-objective optimization (SMOO) framework was developed to enhance the performance of the SMR process under varying biogas feed compositions (Ba-Alawi et al., 2026). The approach combines a multi-input-multi-output deep neural network (MIMO-DNN) with the non-dominated sorting genetic algorithm II (NSGA-II) to analyse different operational scenarios, including constant, moderately varying, and strongly fluctuating methane content in the feed. The effectiveness of the proposed strategy was further confirmed through implementation within a digital twin environment using real biogas data. The results indicated notable improvements, including a reduction in annual operating costs

by 30.59%, a decrease in emissions by 6.68%, and an increase in process efficiency by 22.92%. Despite these promising outcomes, the method is still being refined for full integration with industrial hydrogen production systems. Future research will focus on expanding the dataset to improve model generalization and on developing fully coupled, bidirectional frameworks applicable under real plant operating conditions.

Carbon dioxide–reduced hydrogen can be produced through several approaches, including sorption-enhanced steam methane reforming (SE-SMR), which generates separate high-purity streams of H_2 and CO_2. For this process, ANN and random forest (RF)–based soft sensor models were developed to predict hydrogen production (Nkulikiyinka et al., 2020). Both models demonstrated strong predictive capabilities for gas concentrations in the reformer and regenerator reactors, particularly for species present at high concentrations. Additionally, CH_4 conversion within the reformer was accurately predicted, providing a reliable measure of the reaction efficiency under the tested operating conditions.

ANNs were employed to address a multifactorial, multiobjective optimization problem and to analyse extensive empirical datasets (Arcotumapathy et al., 2012). The methodology involved a Fibonacci-based approach to determine the optimal number of neurons for the ANN architecture, followed by a novel weighted combination of statistically selected candidate ANN models evaluated in a multi-error framework. Data from 200 catalytic SMR cases were used to validate the accuracy and robustness of this integrated ANN modelling approach. The results not only aligned with existing qualitative knowledge but also revealed previously underappreciated factors that could guide improvements in hydrocarbon reforming reactor technology and catalyst design. Notably, the study highlighted that small additions of boron, cerium, or similar metals (below 1 wt.%) to Ni-based catalysts, as well as the use of SBA-15 as a support instead of γ-alumina, can significantly enhance catalytic performance.

A hybrid quantum neural network (QNN)-ANN model was developed to predict the performance of the DRM process (Roh et al., 2024). QNNs offer higher prediction accuracy than traditional machine learning models, including ANNs, even when limited datasets are available. Catalyst datasets for the DRM reaction, drawn from both literature and in-house experiments, were used to benchmark the hybrid QNN against conventional ANN models. The results demonstrated that the hybrid QNN achieved superior prediction accuracy and faster convergence compared to the ANN. This study not only provides a methodological framework for implementing hybrid QNN models but also offers interpretive insights into their operation. The findings underscore the potential of hybrid QNNs as powerful tools for addressing complex problems in catalysis and chemistry, particularly in areas where limited data have historically constrained the application of classical machine learning approaches.

ANNs were applied to develop empirical models for predicting hydrogen yield and providing insights for improving DRM processes over nickel-based catalysts under varying operating and physical conditions (Rahman and Biswas, 2024). The model inputs included temperature, gas velocity, and three key geometric characteristics of the nickel catalysts, enabling prediction of hydrogen production from methane. The ANN was trained using three algorithms: Levenberg-Marquardt, Bayesian regularization, and scaled conjugate gradient, with the best model performance achieved using the Levenberg-Marquardt method. Accurate hydrogen yield predictions were obtained when the network employed the optimal number of hidden neurons and appropriate learning algorithm. This approach allows precise forecasting of catalyst performance based on physical properties, promoting more consistent and reliable DRM reactor operation. However, the study did not consider the effects of catalytic support, catalyst preparation methods, or coke formation on overall activity.

An advanced convolutional neural network (CNN) framework was designed to predict hydrogen yield and carbon monoxide concentration during reforming processes involving methane, methanol, and diesel (Yalcin et al., 2024). In addition, the model was adapted to estimate methane conversion in methane reforming systems. The proposed approach integrates both 2D- and 3D-CNN architectures to improve predictive capability. The results demonstrate that this hybrid CNN model outperforms conventional CNN structures as well as other artificial intelligence methods in estimating key performance indicators of reforming processes. Furthermore, the model enables reliable prediction of critical output variables across different fuel types, highlighting its versatility. Overall, the proposed methodology enhances the accuracy of process performance estimation and provides a robust tool for analysing reforming systems involving various feedstocks.

5. CONCLUSIONS

ANNs are effective tools for modelling methane thermochemical conversion, capturing complex relationships that conventional kinetic models struggle to describe. They have been successfully applied to predict methane conversion, hydrogen yield, syngas composition, and reactor performance.

MLPs remain the most widely used architecture due to their flexibility and reliability. Other architectures, such as RBF networks, CNN and PINN models, show promise for specific tasks, including catalyst coking, dynamic reactor behaviour, and multi-output predictions, although their use is still limited. The choice of ANN depends on dataset size, dimensionality, and the modelling goal, with simpler networks sufficient for basic predictions and more complex models needed for dynamic or multi-output systems.

Data quality and availability are critical. Large experimental or simulation-generated datasets allow for deeper net-

works and better predictions, while small datasets increase the risk of overfitting. Input selection, from operating conditions to catalyst properties and time-dependent variables, is also key to capturing system dynamics accurately.

Recent trends are moving toward integrated frameworks that combine ANNs with first-principles physical knowledge and advanced simulations. Hybrid models, as well as physics-informed or physics-enhanced networks, improve predictive accuracy, enforce physical consistency, and increase interpretability. Such approaches are expected to play a central role in designing efficient reactors, optimizing catalysts, and advancing hydrogen and syngas production technologies.

ACKNOWLEDGEMENTS

This work is related to the TITAN project (No. 101069474) funded by the European Union (HORIZON EUROPE Climate, Energy and Mobility). Views and opinions expressed are however those of the authors only and do not necessarily reflect those of the European Union or the European Climate, Infrastructure and Environment Executive Agency (CINEA). Neither the European Union nor the granting authority can be held responsible for them.

REFERENCES

Abedini F., Hosseini S.A., Niaei A., Salari D., Abbasi M., Marmarshahi S., 2018. Design and optimization of new $La_{1-x}Ce_xNi_{1-y}Fe_yO_3$ (x, y = 0–0.4) nano catalysts in dry reforming of methane. *Int. J. Green Energy*, 15, 20–27. DOI: 10.1080/15435075.2017.1405813.

Adhikari S., Fernando S., Gwaltney S.R., To S.D.F., Bricka R.M., Steele P.H., Haryanto A., 2007. A thermodynamic analysis of hydrogen production by steam reforming of glycerol. *Int. J. Hydrogen Energy*, 32, 2875–2880. DOI: 10.1016/j.ijhydene.2007.03.023.

Ahmad K., Jaoude M.A., Bankole A.A., Polychronopoulou K., 2025. Hydrogen production towards carbon-free economy: a comprehensive thermodynamic analysis. *Energy Convers. Manage.*, 326, 119492. DOI: 10.1016/j.enconman.2025.119492.

Ahmad K., Polychronopoulou K., Abi Jaoude M., 2022. CH_4 valorisation reactions: a comparative thermodynamic analysis and their limitations. *Fuel*, 320, 123877. DOI: 10.1016/j.fuel.2022.123877.

Alsaffar M.A., Ayodele B.V., Mustapa S.I., 2020. Scavenging carbon deposition on alumina supported cobalt catalyst during renewable hydrogen-rich syngas production by methane dry reforming using artificial intelligence modeling technique. *J. Cleaner Prod.*, 247, 119168. DOI: 10.1016/j.jclepro.2019.119168.

Arcotumapathy V., Siahvashi A., Adesina A.A., 2012. A new weighted optimal combination of ANNs for catalyst design and reactor operation: methane steam reforming studies. *AIChE J.*, 58, 2412–2427. DOI: 10.1002/aic.12748.

Ayodele B.V., Cheng C.K., 2015. Modelling and optimization of syngas production from methane dry reforming over ceria-supported cobalt catalyst using artificial neural networks and Box–Behnken design. *J. Ind. Eng. Chem.*, 32, 246–258. DOI: 10.1016/j.jiec.2015.08.021.

Ayodele B.V., Mustapa S.I., Alsaffar M.A., Cheng C.K., 2019. Artificial intelligence modelling approach for the prediction of CO-rich hydrogen production rate from methane dry reforming. *Catalysts*, 9, 738. DOI: 10.3390/catal9090738.

Ba-Alawi A.H., Chung H., Kim J., 2026. A rule-based digital twin strategy for optimizing hydrogen production from biogas under dynamic feed conditions. *Energy*, 342, 139779. DOI: 10.1016/j.energy.2025.139779.

Biermann F., Uglietti R., Döppel F.A., Kircher T., Bracconi M., Maestri M., Votsmeier M., 2025. Enabling micro-kinetics based simulation of industrial packed-bed reactors by physics-enhanced neural networks. *Chem. Eng. J.*, 519, 163598. DOI: 10.1016/j.cej.2025.163598.

Carranza-Abaid A., Svendsen H.F., Jakobsen J.P., 2023. Thermodynamically consistent vapor-liquid equilibrium modelling with artificial neural networks. *Fluid Phase Equilib.*, 564, 113597. DOI: 10.1016/j.fluid.2022.113597.

Cherbański R., Kotkowski T., Murgrabia S., Molga E., Stankiewicz A., 2026a. ANN-based prediction of equilibrium gas composition and carbon yield in methane pyrolysis and reforming methods. *React. Chem. Eng.*, 11, 691–706. DOI: 10.1039/D5RE00322A.

Cherbański R., Murgrabia S., Molga E., Stankiewicz A., Kotkowski T., 2026b. Forecasting temporal profiles of Fe/C catalyst coking in methane pyrolysis via moving window neural networks. DOI:

Ciou S.-J., Jhang Y.-W., Lai Y.-J., Kuan-Zong F., Hung M.-H., Chiang K.-W., 2007. A neural network model in $LaNi_xAl_{1-x}O_3$ catalyst for methane reforming in SOFC. *ECS Trans.*, 7, 1929. DOI: 10.1149/1.2729305.

Cybenko G., 1989. Approximation by superpositions of a sigmoidal function. *Math. Control Signals Syst.*, 2, 303–314. DOI: 10.1007/BF02551274.

de Souza P.A.L., Afzal R.M., Camacho F.G., Mahinpey N., 2025. Catalyst development for the tri-reforming of methane (TRM) process by integrated singular machine learning models. *Can. J. Chem. Eng.*, 103, 758–770. DOI: 10.1002/cjce.25397.

Del-Mazo-Alvarado O., Bonilla-Petriciolet A., 2022. Assessment of the simultaneous regression of liquid-liquid and vapor-liquid equilibria data of binary systems using NRTL and artificial neural networks. *Fluid Phase Equilib.*, 561, 113537. DOI: 10.1016/j.fluid.2022.113537.

Demidov D.V., Mishin I.V., Mikhailov M.N., 2011. Gibbs free energy minimization as a way to optimize the combined steam and carbon dioxide reforming of methane. *Int. J. Hydrogen Energy*, 36, 5941–5950. DOI: 10.1016/j.ijhydene.2011.02.053.

Di Nardo A., Portarapillo M., Russo D., Di Benedetto A., 2024. Hydrogen production via steam reforming of different fuels: thermodynamic comparison. *Int. J. Hydrogen Energy*, 55, 1143–1160. DOI: 10.1016/j.ijhydene.2023.11.215.

European Environmental Agency, 2025. *Total net greenhouse gas emission trends and projections in Europe*. Available at: https://www.eea.europa.eu/en/analysis/indicators/total-greenhouse-gas-emission-trends.

Fang R., Zhou T., Xu Z., Hu X., Zhang M., Yang H., 2025. Energy-efficient prediction of carbon deposition in DRM processes through optimized neural network modeling. *Energies*, 18, 3172. DOI: 10.3390/en18123172.

Faungnawakij K., Kikuchi R., Eguchi K., 2006. Thermodynamic evaluation of methanol steam reforming for hydrogen production. *J. Power Sources*, 161, 87–94. DOI: 10.1016/j.jpowsour.2006.04.091.

Gadalla A.M., Bower B., 1988. The role of catalyst support on the activity of nickel for reforming methane with CO_2. *Chem. Eng. Sci.*, 43, 3049–3062. DOI: 10.1016/0009-2509(88)80058-7.

Gendy T.S., El-Salamony R.A., Alrashed M.M., Bentalib A., Osman A.I., Kumar R., Fakeeha A.H., Al-Fatesh A.S., 2024. Enhanced predictive optimization of methane dry reforming via Response Surface methodology and artificial neural network approaches: Insights using a novel nickel-strontium-zirconium-aluminum catalyst. *Mol. Catal.*, 562, 114216. DOI: 10.1016/j.mcat.2024.114216.

Guéret C., Daroux M., Billaud F., 1997. Methane pyrolysis: thermodynamics. *Chem. Eng. Sci.*, 52, 815–827. DOI: 10.1016/S0009-2509(96)00444-7.

Hornik K., Stinchcombe M., White H., 1989. Multilayer feedforward networks are universal approximators. *Neural Networks*, 2, 359–366. DOI: 10.1016/0893-6080(89)90020-8.

Hossain M.A., Ayodele B.V., Cheng C.K., Khan M.R., 2016. Artificial neural network modeling of hydrogen-rich syngas production from methane dry reforming over novel $Ni/CaFe_2O_4$ catalysts. *Int. J. Hydrogen Energy*, 41, 11119–11130. DOI: 10.1016/j.ijhydene.2016.04.034.

Igwegbe C.A., Adeniyi A.G., Ighalo J.O., 2021. ANN modelling of the steam reforming of naphthalene based on non-stoichiometric thermodynamic analysis. *Chem. Pap.*, 75, 3363–3372. DOI: 10.1007/s11696-021-01566-2.

Ismaila A., Chen X., Gao X., Fan X., 2021. Thermodynamic analysis of steam reforming of glycerol for hydrogen production at atmospheric pressure. *Front. Chem. Sci. Eng.*, 15, 60–71. DOI: 10.1007/s11705-020-1975-0.

Jabbour K., 2020. Tuning combined steam and dry reforming of methane for "metgas" production: a thermodynamic approach and state-of-the-art catalysts. *J. Energy Chem.*, 48, 54–91. DOI: 10.1016/j.jechem.2019.12.017.

Jafarizadeh A., Panjepour M., Emami M.D., 2024. Advanced modelling and optimization of steam methane reforming: from CFD simulation to machine learning – driven optimization. *Int. J. Hydrogen Energy*, 96, 1262–1280. DOI: 10.1016/j.ijhydene.2024.11.352.

Jensen C., Duyar M.S., 2021. Thermodynamic analysis of dry reforming of methane for valorization of landfill gas and natural gas. *Energy Technol.*, 9, 2100106. DOI: 10.1002/ente.202100106.

Kumbhat A., Madaan A., Goel R., Appari S., Al-Fatesh A.S., Osman A.I., 2024. Predicting nickel catalyst deactivation in biogas steam and dry reforming for hydrogen production using machine learning. *Process Saf. Environ. Prot.*, 191, 1833–1846. DOI: 10.1016/j.psep.2024.09.020.

L'hospital V., de Araujo L.G., Landrivon E., Mello A., Radoiu M., Trillaud V., Meunier J.-F., Schuurman Y., Guilhaume N., Farrusseng D., 2025. Methane pyrolysis into hydrogen and solid carbon: a comparative analysis of conventional and microwave heating approaches. *Catal. Today*, 459, 115430. DOI: 10.1016/j.cattod.2025.115430.

L'hospital V., de Araujo L.G., Schuurman Y., Guilhaume N., Farrusseng D., 2024. Direct biogas reforming to turquoise H_2 and carbon material in a catalytic fluidised-bed reactor. *New J. Chem.*, 48, 9656–9662. DOI: 10.1039/D4NJ00846D.

Lima da Silva A., Malfatti C.D.F., Müller I.L., 2009. Thermodynamic analysis of ethanol steam reforming using Gibbs energy minimization method: a detailed study of the conditions of carbon deposition. *Int. J. Hydrogen Energy*, 34, 4321–4330. DOI: 10.1016/j.ijhydene.2009.03.029.

Morlanés N., Lezcano G., Yerrayya A., Mazumder J., Castaño P., 2022. Improving robustness of kinetic models for steam reforming based on artificial neural networks and ab initio calculations. *Chem. Eng. J.*, 433, 133201. DOI: 10.1016/j.cej.2021.133201.

Nguyen V.D., Tan R.R., Brondial Y., Fuchino T., 2007. Prediction of vapor–liquid equilibrium data for ternary systems using artificial neural networks. *Fluid Phase Equilib.*, 254, 188–197. DOI: 10.1016/j.fluid.2007.03.014.

Nkulikiyinka P., Yan Y., Güleç F., Manovic V., Clough P.T., 2020. Prediction of sorption enhanced steam methane reforming products from machine learning based soft-sensor models. *Energy AI*, 2, 100037. DOI: 10.1016/j.egyai.2020.100037.

Piotrowski K., Piotrowski J., Schlesinger J., 2003. Modelling of complex liquid–vapour equilibria in the urea synthesis process with the use of artificial neural network. *Chem. Eng. Process. Process Intensif.*, 42, 285–289. DOI: 10.1016/S0255-2701(02)00060-0.

Pizoń Z., Kimijima S., Brus G., 2024a. Enhancing a deep learning model for the steam reforming process using data augmentation techniques. *Energies*, 17, 2413. DOI: 10.3390/en17102413.

Pizoń Z., Kimijima S., Brus G., 2024b. Integrating experimental and numerical data for improved steam reforming simulation with deep learning. *J. Phys. Conf. Ser.*, 2812, 012024. DOI: 10.1088/1742-6596/2812/1/012024.

Pizoń Z., Kimijima S., Brus G., 2025. Bridging equilibrium and kinetics prediction with a data-weighted neural network model of methane steam reforming. *Int. J. Hydrogen Energy*, 175, 151367. DOI: 10.1016/j.ijhydene.2025.151367.

Rahman M.H., Biswas M., 2024. Modeling of dry reforming of methane using artificial neural networks. *Hydrogen*, 5, 800–818. DOI: 10.3390/hydrogen5040042.

Reynel-Ávila H.E., Bonilla-Petriciolet A., Tapia-Picazo J.C., 2019. An artificial neural network-based NRTL model for simulating liquid-liquid equilibria of systems present in biofuels production. *Fluid Phase Equilib.*, 483, 153–164. DOI: 10.1016/j.fluid.2018.11.009.

Roh J., Oh S., Lee D., Joo C., Park J., Moon I., Ro I., Kim J., 2024. Hybrid quantum neural network model with catalyst experimental validation: application for the dry reforming of methane. *ACS Sustainable Chem. Eng.*, 12, 4121–4131. DOI: 10.1021/acssuschemeng.3c07496.

Rossi C.C.R.S., Alonso C.G., Antunes O.A.C., Guirardello R., Cardozo-Filho L., 2009. Thermodynamic analysis of steam reforming of ethanol and glycerine for hydrogen production. *Int. J. Hydrogen Energy*, 34, 323–332. DOI: 10.1016/j.ijhydene.2008.09.071.

Samris A., Naanani H., Nachtane M., Faik A., 2025. A physics-informed deep learning framework for enhanced hydrogen production via electrified steam methane reforming. *Int. J. Hydrogen Energy*, 193, 152376. DOI: 10.1016/j.ijhydene.2025.152376.

Sánchez-Bastardo N., Schlögl R., Ruland H., 2021. Methane pyrolysis for zero-emission hydrogen production: a potential bridge technology from fossil fuels to a renewable and sustainable hydrogen economy. *Ind. Eng. Chem. Res.*, 60, 11855–11881. DOI: 10.1021/acs.iecr.1c01679.

Shabbar S., Janajreh I., 2013. Thermodynamic equilibrium analysis of coal gasification using Gibbs energy minimization method. *Energy Convers. Manage.*, 65, 755–763. DOI: 10.1016/j.enconman.2012.02.032.

Shahid M.I., Farhan M., Rao A., Li W., Salam H.A., Xiao Q., Chen T., Li X., Ma F., 2025. Effect of methane/water flowrate on waste heat recovery and hydrogen production by steam methane reforming process and predicted by artificial neural network (ANN). *Energy*, 331, 136877. DOI: 10.1016/j.energy.2025.136877.

Soltanimehr S., Rahimpour M.R., Shariati A., 2026. Integrated artificial intelligence modelling and multi objective optimization to optimize an industrial auto-thermal reformer. *Energy Convers. Manage.*, 349, 120831. DOI: 10.1016/j.enconman.2025.120831.

Taherian Z., Yousefpour M., Tajally M., Khoshandam B., 2017. Catalytic performance of Samaria-promoted Ni and Co/SBA-15 catalysts for dry reforming of methane. *Int. J. Hydrogen Energy*, 42, 24811–24822. DOI: 10.1016/j.ijhydene.2017.08.080.

Vo N.D., Oh D.H., Hong S.-H., Oh M., Lee C.-H., 2019. Combined approach using mathematical modelling and artificial neural network for chemical industries: steam methane reformer. *Appl. Energy*, 255, 113809. DOI: 10.1016/j.apenergy.2019.113809.

Xu J., Froment G.F., 1989. Methane steam reforming, methanation and water-gas shift: I. Intrinsic kinetics. *AIChE J.*, 35, 88–96. DOI: 10.1002/aic.690350109.

Yalcin S., Yildirim M., Alatas B., 2024. Advanced convolutional neural network modeling for fuel cell system optimization and efficiency in methane, methanol, and diesel reforming. *PeerJ Comput. Sci.*, 10, e2113. DOI: 10.7717/peerj-cs.2113.

Zamaniyan A., Joda F., Behroozsarand A., Ebrahimi H., 2013. Application of artificial neural networks (ANN) for modeling of industrial hydrogen plant. *Int. J. Hydrogen Energy*, 38, 6289–6297. DOI: 10.1016/j.ijhydene.2013.02.136.

Zhu J., Zhang D., King K.D., 2001. Reforming of CH_4 by partial oxidation: thermodynamic and kinetic analysis. *Fuel*, 80, 899–905. DOI: 10.1016/S0016-2361(00)00165-7

Chemical Engineering Horizons and Perspectives.
Article series endorsed by the Scientific Committee on Chemical and Process Engineering
of the Polish Academy of Sciences, term 2024–2027